# Assimilation of High Resolution Mode-S Wind and Temperature Observations in a Limited Area NWP-model

Siebren de Haan and Ad Stoffelen

# Contents

**Abstract**

In this report we present the positive impact of high resolution (in space and time) of wind and temperature observation from aircraft on short-range numerical weather forecasting. The observations are retrieved using the Tracking and Ranging radar from Air-traffic Control at Schiphol Airport, the Netherlands. This enhanced surveillance radar tracks all aircraft in sight every four seconds generating one million wind and temperature observations per day around the Netherlands.

When assimilated into a numerical model with a hourly update cycle, the three dimensional wind field is better for now-casting purposes than the operational forecast which is available every three hours. The positive impact on wind in the first hours of the forecast gradually turns into a neutral impact, when compared to other wind and temperature observations. The gain for now-casting comes from the short latency of the forecasts combined with the high resolution of the observations.

All in all, assimilation of high resolution wind (and temperature) observations is therefore benificial for now-casting and short-range forecasts up to two to three hours.

# Chapter 1

# Introduction

Advances in meso-scale numerical weather prediction are very relevant for nowcasting and short-range forecasting of, among others, extreme weather events. Of particular concern is the initialisation of such models on small scales through the assimilation of a set of high-resolution observations that is fit for this purpose. Not only is higher spatial density required for analysing small scales, but moreover these scales develop relatively fast, thus requiring timely observations at high temporal density. Furthermore, to specify the atmospheric dynamics, wind observations are the most important for meso-scale numerical weather prediction (NWP). Most notably, high resolution upper air profile observations are lacking (Stoffelen et al., 2006; WMO, 2004, 2006). An improvement of the initial wind field will result in a better forecast of both wind and temperature. Temperature on the contrary is a large scale parameter and is thus of less importance for meso-scale numerical weather prediction. Nevertheless, temperature plays an important role in meso-scale development; the lid on the planetary boudnary layer, which inhibits convections is mainly temperature profile dependent.

Accurate forecasts of wind, temperature and humidity are important for forecasting severe weather. In particular, aviation highly depends on meteorological information for safety. Furthermore, improved forecasts will also be beneficial for air traffic control, especially in case of so-called "green landings". These continuous descent approaches will save fuel and decrease noise pollution in the neighbourhood of the airport.

Radiosonde and aircraft are the main sources of upper air wind WMO (2008), temperature and humidity. The aircraft data used at KNMI is collected through the AMDAR (Aircraft Meteorological Data Relay) system. In this report we will exploit another source of upper air atmospheric wind and temperature information from aircraft. Benjamin et al. (1991) showed that in the Rapid Update Cycle (RUC) on a three-hour cycle from the National Centers for Environmental Prediction (NCEP) aircraft data lead to significant improvements in 3- and 6-h forecasts. Wind errors were reduced by approximately 10%.

The radiosonde network has been optimized for benificial impact in synoptic NWP. For meso-scale meteorological applications shortcomings in the radiosonde network exist in both horizontal and temporal sampling. The horizontal sampling over land is approximately 500 km, while over the oceans only a few automatic radiosondes are lauched, while the temperoral sampling is 6 to 12 hours.

AMDAR is the most important data source for winds over the Atlantic Ocean, and the second most important data source after radiosondes over North America in the UK MetOffice model (Graham et al., 2000). Moninger et al. (2003) showed also that AMDAR data improve both the short- and the long-term weather forecasts. In Moninger et al. (2009) multi-year evaluation of Tropospheric AMDAR (TAMDAR) showed a positive impact on 3 hour RUC forecasts of temperature, relative humidity, and wind. Recent assimilation experiments (Benjamin et al., 2010) were performed with eight different observation data types. Assimilation experiments in the hourly RUC, showed that aircraft observations had the largest overall impact on the forecast quality.

Only recently a method to retrieve wind and temperature information from all aircraft in the vicinity of a tracking and ranging (TAR-1) radar has been developed (De Haan, 2009). Using TAR-1 radar data of the air-traffic control at Schiphol airport, De Haan (2009) showed that the wind information from this source has a quality comparable to AMDAR wind. Temperature information can also inferred from TAR, however the quality of these observations is lower than the AMDAR. These observations are gathered using the Selective Mode of the radar, and are therefore called Mode-S observations.

In this report we show the impact of high resolution wind (and temperature) observations from aircraft by assimilation into the HIRLAM NWP model (Undén et al., 2002). All aircraft within the range of the radar are polled and can be used to derive wind and temperature observations. The range of the radar is about 275 km The observations are recorded with a frequency of every four seconds and accumulated into batches of 10 minutes, with typically 10,000 to 16,000 observations, becoming available with almost no latency.

The impact is assessed by performing NWP experiments without and with the Mode-S data in the HIRLAM NWP model, close to the operational configuration. An hourly assimilation cycle will be applied to exploit the high resolution (in space and time) of these new observations. Although all experiments are performed off-line, the settings, data sources, boundaries, etc., are kept as close as possible to operational practice to have an assessment of the impact of these observations representative for operational practice.

The high resolution in both the temporal and spatial domain of these observation opens the path to high resolution data assimilation. Moreover, the fast availability can be exploited by a rapid update cycle of one hour (or even 15 minutes). This may trigger now-casting applications using a NWP model.

## 1.1 Outline

This report is ordered as follows. We will start with the description of the numerical weather prediction model used in this study. Next we will describe the observations used in the assimilation experiments. A description of the general weather situation during the experiment from February 1, 2008, to March 10, 2008 , is given in next section. This is followed by the results of the experiments and a discussing of impact on selected cases. The final sections are devoted to the conclusions and recommendations.

# Chapter 2

# Observations and Weather Situation

In this chapter the observations used in the assimilation experiments are discussed. In the current operational version of HIRLAM, only surface pressure observations, radiosonde (wind, temperature and humidity) observations and AMDAR (wind and temperature) observations are used. These are discussed briefly below, together with the Mode-S observations. The period under consideration runs from the first of February 2008 to March, 10 2008. The last section is devoted to a overview of the synoptic weather situation in this period.

## 2.1 Aircraft observations

Aircraft are equipped with sensors which measure the speed of the aircraft, its position and ambient temperature and pressure. Wind information can be derived from these measurements. At present, a selection of these observations are transmitted to a ground station using the AMDAR (Aircraft Meteorological Data Relay) system. An atmospheric profile can be generated when measurements are taken during takeoff and landing. See WMO (2003); De Haan (2009) for more details.

A new type of aircraft related meteorological information stems from the observations inferred from a tracking and ranging radar used for air traffic control. This data is called Mode-S (because it is using the surveillance mode of the radar). Wind information for AMDAR and Mode-S is derived from the position of the aircraft reported by heading, ground track and true air speed $\mathbf{V}_t$. The wind vector $\mathbf{V}$ is the difference between the motion of the aircraft relative to the ground and its motion relative to the air. Thus $\mathbf{V}$ is the difference in heading vector $\mathbf{V}_t$, defined by length $V_t$ and heading $\alpha_t$, and the ground track vector $\mathbf{V}_f$, defined by length $V_g$ and angle $\alpha_g$, that is

$$\mathbf{V} = \mathbf{V}_g - \mathbf{V}_t. \tag{2.1}$$

AMDAR temperature is obtained from direct readings of the sensors on-board of the aircraft, while Mode-S temperature is inferred from the reported Mach number, true air speed and flight level (which is directly related to pressure). The relation between speed of sound and temperature and the ideal gas law are used to estimate the air temperature $T$ as follows

$$T = 2.4923 \cdot 10^{-3} V_t^2 \, M^{-2}, \tag{2.2}$$

where $T$ is in K. The Mach-number $M$ has no dimension. The vertical coordinate of aircraft observations is is also expressed in flight levels, which the pressure (altitude) divided by 30.48. For example FL100 is at pressure 696 hPa, FL200 at 465 hPa, FL300 at 300 hPa and FL400 at 187 hPa (approximately).

In De Haan (2009) it was shown that, when corrections and calibration on these observations are applied good quality wind observations can be obtained. After applying the corrections and calibration, the wind observations from Mode-S are of nearly the same quality as the wind observations from AMDAR (typically an RMS of 2 to 3.5 m/s, depending on height). The temperature observations are of worse quality as compared to AMDAR. Below, we discuss the observation density of AMDAR and Mode-S during the experiment period.

### 2.1.1 AMDAR Observations

AMDAR uses raw data available from the aircraft monitoring systems. Data rates typically vary from one sample per second to 16 samples per second. According to WMO (2003) in order to reduce the noise, the AMDAR reports are averages of observations over a certain time depending on the phase of flight. This averaging is done internally by the aircraft computer before transmitting the data with averaging times for ascent and descent of 10s and for level flight above flight level FL200 (20 000 ft or 465hPa) of 30s.

The availability of AMDAR data depends on the phase of flight. For level flight an observation frequency is usually once every 7 minutes. In case of a "maximum wind event" an extra observation is made. For an ascending aircraft, observations are made at nine intervals of 10 hPa (or 19 intervals of 5 hPa), followed by pressure observation interval of 50 hPa (or 25 hPa) until a height of 465hPa is reached (FL200). For a descending plane, the first observation is made at 500hPa, pressure intervals are set to 50hPa (or optionally 25 hPa) until 700 hPa is reached. From 700hPa onwards the pressure observation interval is set to 10hPa (or 5 hPa), see WMO (2003) for the details.

The coverage of AMDAR observations show the main flight routes, see Figure 2.1. The observations are concentrated around the main airports, such as London (Heathrow), Paris and Frankfurt.

Although Schiphol airport is also one of the main airports in Europe, the number of observations is limited. This is due to the choices made by the EUMETNET-AMDAR team based on the costs different airlines charge for the observations: Lufthansa and SAS are cheaper than KLM. In Figure 2.2 the distribution of the AMDAR observations are calculated for nine regions in the mid-western part of Europe. The number of AMDAR observations differ substantially between the regions. Furthermore, the distribution over the day is different. For example, the lower-left region (the most western part of France) has 1800 observation around 6 UTC, while the rest of the day only at 14 and 19 UTC around 600 observations are present. Germany is covered well, also in the vertical. Note also that for all regions very little observations are performed between 0 and 5 UTC.

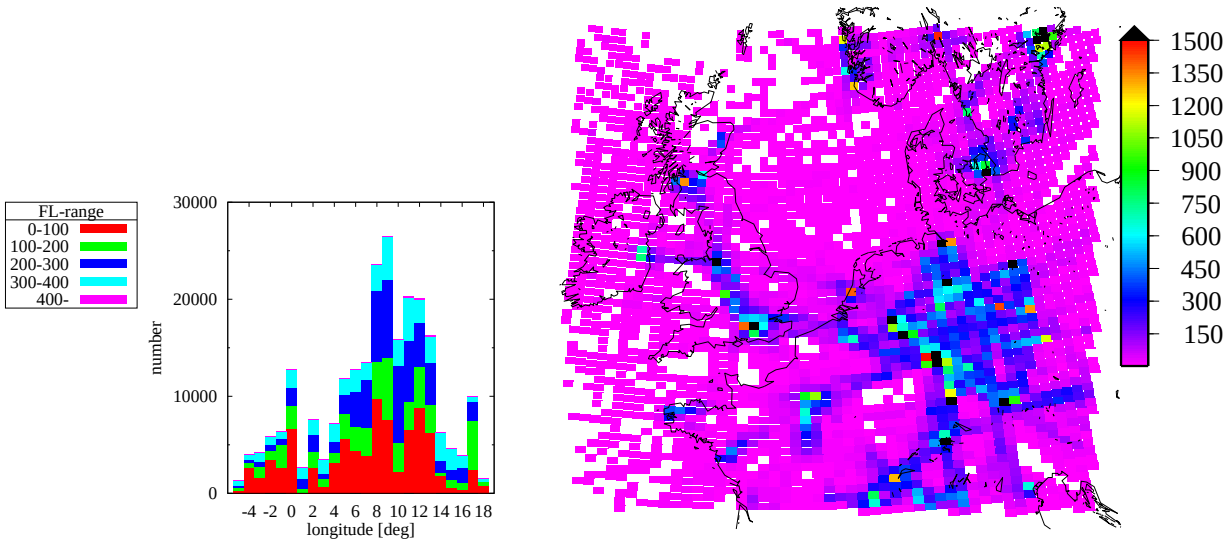


Figure 2.1: Coverage and number of AMDAR observations for the period 01/02/2008-10/03/2008.

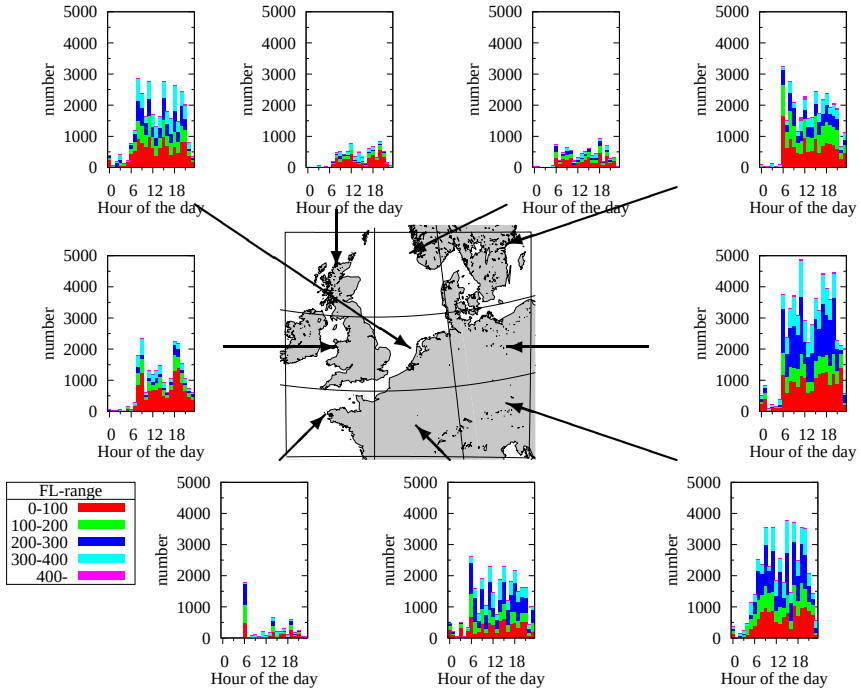


Figure 2.2: Vertical coverage of AMDAR observations in the period 01/02/2008 - 10/03/2008 for nine regions.

### 2.1.2 Mode-S Observations

Mode-S data used in this report are collected using the tracking and ranging radar (TAR-1) at Amsterdam Schiphol (EHAM) airport. In response to a request by the radar each individual

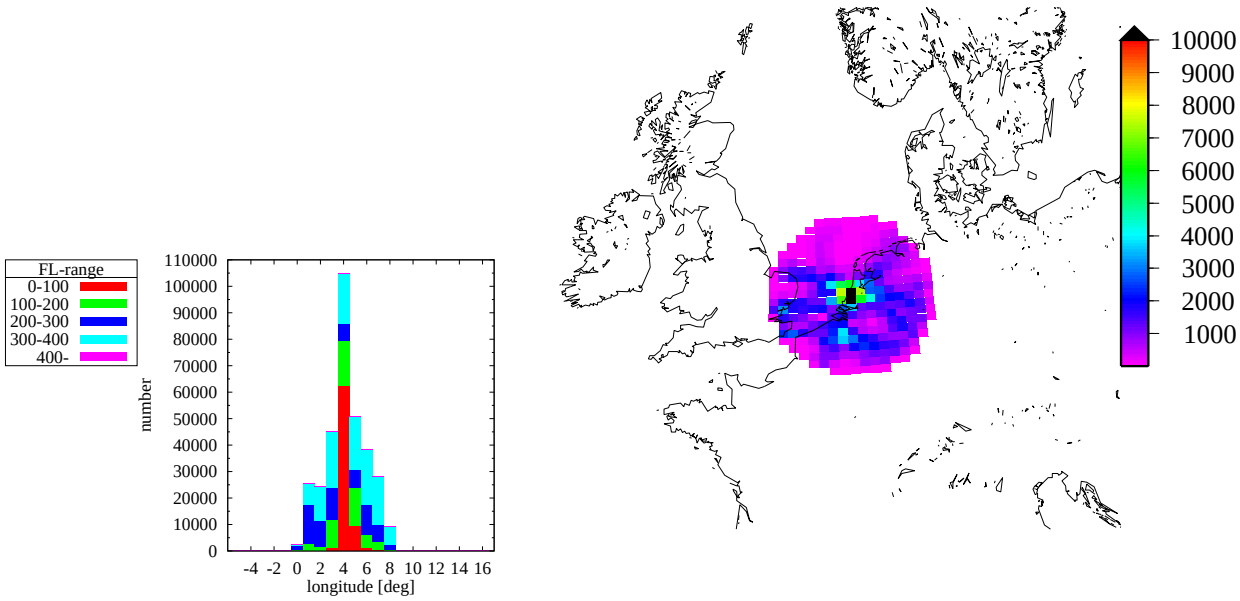


Figure 2.3: Number of Mode-S observations available for assimilation in the period from 1 Feb. to 10 March.

aircraft sends information on the current speed and heading and Mach-number, from which temperature and wind can be inferred. The radar performs a full scan every four seconds and the area covered is 270 km around the radar. The coverage is limited by the curvature of the earth. The recorded messages contain information generated by the flight computer including the transponder-id, flight level, Mach-number, roll, true airspeed and heading. The message is complemented with information on the position and ground track from the tracking radar. All aircraft are queried, resulting in about $1.5 \cdot 10^6$ observations per day around Amsterdam Schiphol.

Wind speed and direction are obtained in a similar way as for AMDAR (see Eq. 2.1). As indicated before, temperature observations are inferred from the observed Mach-number, pressure (i.e. the flight level) and true air speed.

The coverage of Mode-S shown in Figure 2.3 immediately exposes the limited range of the observations due to the observation method. However, the number of observations is very large (note the differences in scale between the AMDAR and Mode-S coverage figures) thus potentially capable of observing small and fast scale weather phenomena. The concentration of the observations around Schiphol is clearly visible and also Brussels can be detected from the coverage.

### 2.1.3 Daily Vertical Coverage of Mode-S and AMDAR

The Figure 2.4 shows the daily coverage of the Mode-S and AMDAR observations for five flight level intervals. No Mode-S observations were recorded between 00 and 01 UTC, due to the experimental nature of the TAR1 system in the February-March period. The number of observations in the other early hours is also small due to landing restrictions at nighttime. Note

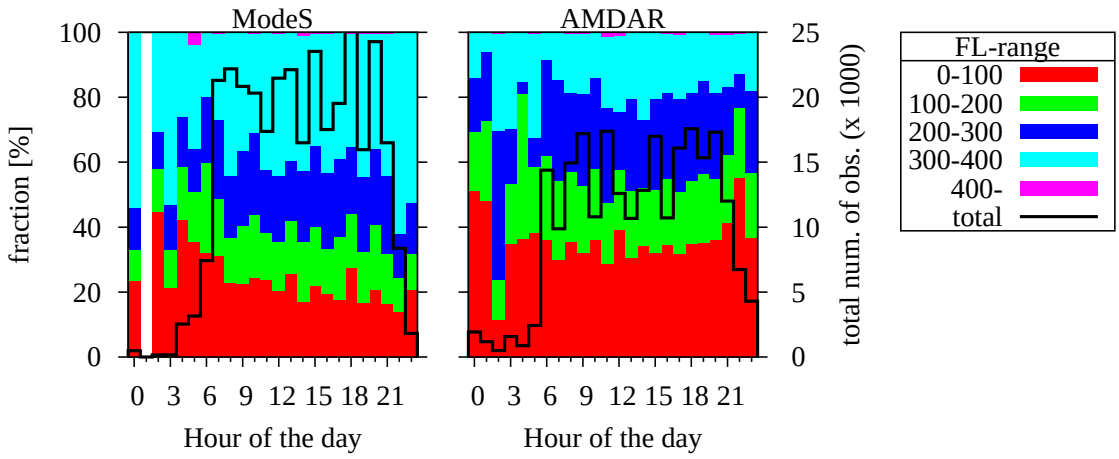


Figure 2.4: Total number of observations and vertical coverage of Mode-S and AMDAR per hour of the day in the period from 01 February to 10 March 2008.

also that very few aircraft are crossing the Netherlands at high altitudes in the early hours. During the rest of the day both AMDAR and Mode-S sample the vertical very well. Mode-S has a different distribution of the observations along the profile; between FL300 and FL400 a higher percentage of observations is made than that for AMDAR possibly due to its conical view and the prescribed observation frequencies of AMDAR. A lot of aircraft depart and arrive at Schiphol between 04 and 08 UTC.

## 2.2 Surface Observations

Every 6 hours the pressure observations from the available SYNOP stations are assimilated. In the Figure 2.5 below the number of used pressure observations are shown in the period 1 February to 10 March. The coverage is mainly restricted to land, with some observations from platforms in the North Sea. Note the synop observations from Denmark Chech Republic and Sweden are not included in the dataset for the whole period.

## 2.3 Radiosonde observations

Radiosondes measure a profile of temperature, wind and humidity. A radiosonde system consists of a ground segment and a balloon to which a small lightweight container is attached. A temperature sensor and humidity sensor are attached to the container. A calibrated pressure sensor and/or a GPS receiver is used to determine the geopotential altitude (and latitude and longitude position in case a GPS is used). The pressure, temperature and humidity information is transmitted to the ground segment where the wind speed and direction are inferred from the ground track of the balloon during its ascent (using LORAN-C or GPS); the rate of ascent is about 18 km/h. The radiosonde is launched approximately 40-50 minutes before the synoptic

hours (which are 00, 06, 12 and 18 UTC) to assure that it reaches the tropopause (i.e. 500 hPa) around the synoptic main hour. Because of the long duration of the flight (approximately 2 hours), this observation method implies that the actual observation time at a certain height does not correspond to the profile timestamp and differ by about an hour. Because of the wind the radiosonde drifts away, the observed profile does not correspond exactly to a profile above the launch site. these differences are small and generally ignored in data assimilation.

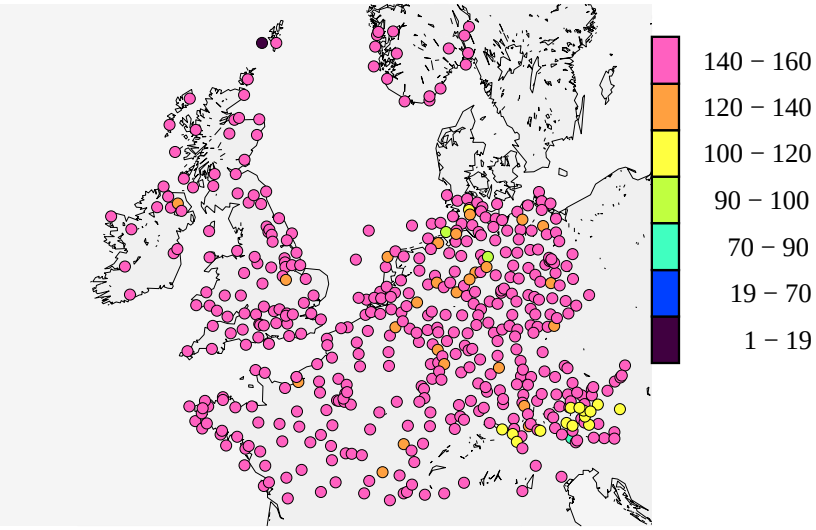


Figure 2.5: Coverage and number of observations assimilated in the period 1 February 2008 to 10 March 2008.

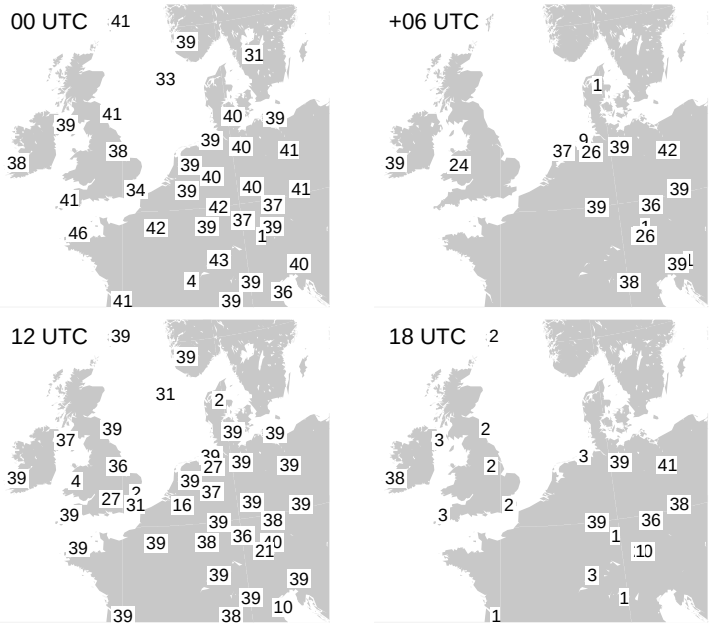


Figure 2.6: Coverage and number of radiosonde observations in the Feb.-Mar. period at four synoptic hours (00, 06, 12 and 18 UTC).

In Figure 2.6 the coverage and number of radiosonde observations for the period 1 Feb. to 10 Mar. is shown for four launch times. The main synoptic hours (00 and 12) show the largest number of launches.

While excellent in the vertical, the distribution of the radiosonde network in Europe is too coarse in time and horizontal coverage for meso-scale modelling. Moreover, the frequency of a large number of radiosonde launches in Europe were reduced from four times per day to two in order to reduce the costs of the total meteorological observing network. Despite the coarse temporal and horizontal resolution, radiosonde observations are a valuable source of information on temperature, humidity, and wind in the atmosphere.

## 2.4 Synoptic Weather Situation

The experiments are run from 01/02/2008 to 10/03/2008. In this period the atmospheric flow displayed consistent variabilities. Figure 2.7 shows the observed surface pressure and temperature, as well as the upper air winds. During the first days of February, a number of fronts passed the Netherlands, as can be seen in Figure 2.8(a), in which the weather analysis is

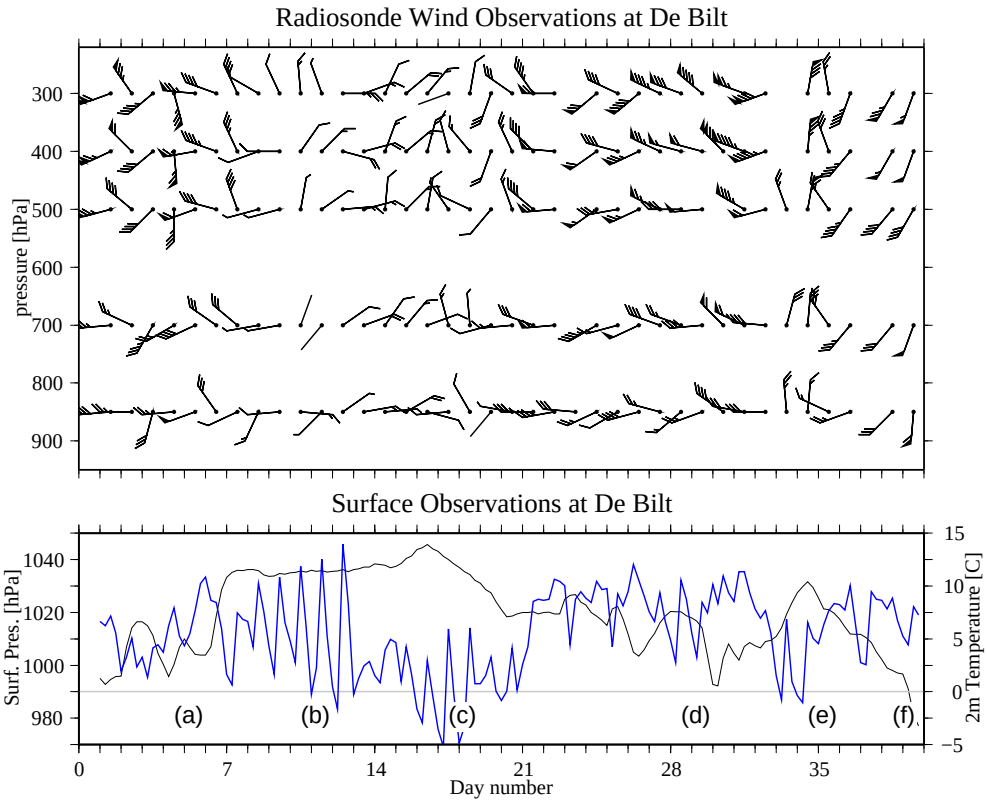


Figure 2.7: Surface and radiosonde observations at De Bilt. Top panel shows the wind speed (in knots) and direction at 12 UTC. Bottom panel shows the pressure (black line) and temperature at the surface observed hourly. The labels (a) to (f) refer to the weather analysis displayed in Figure 2.8.

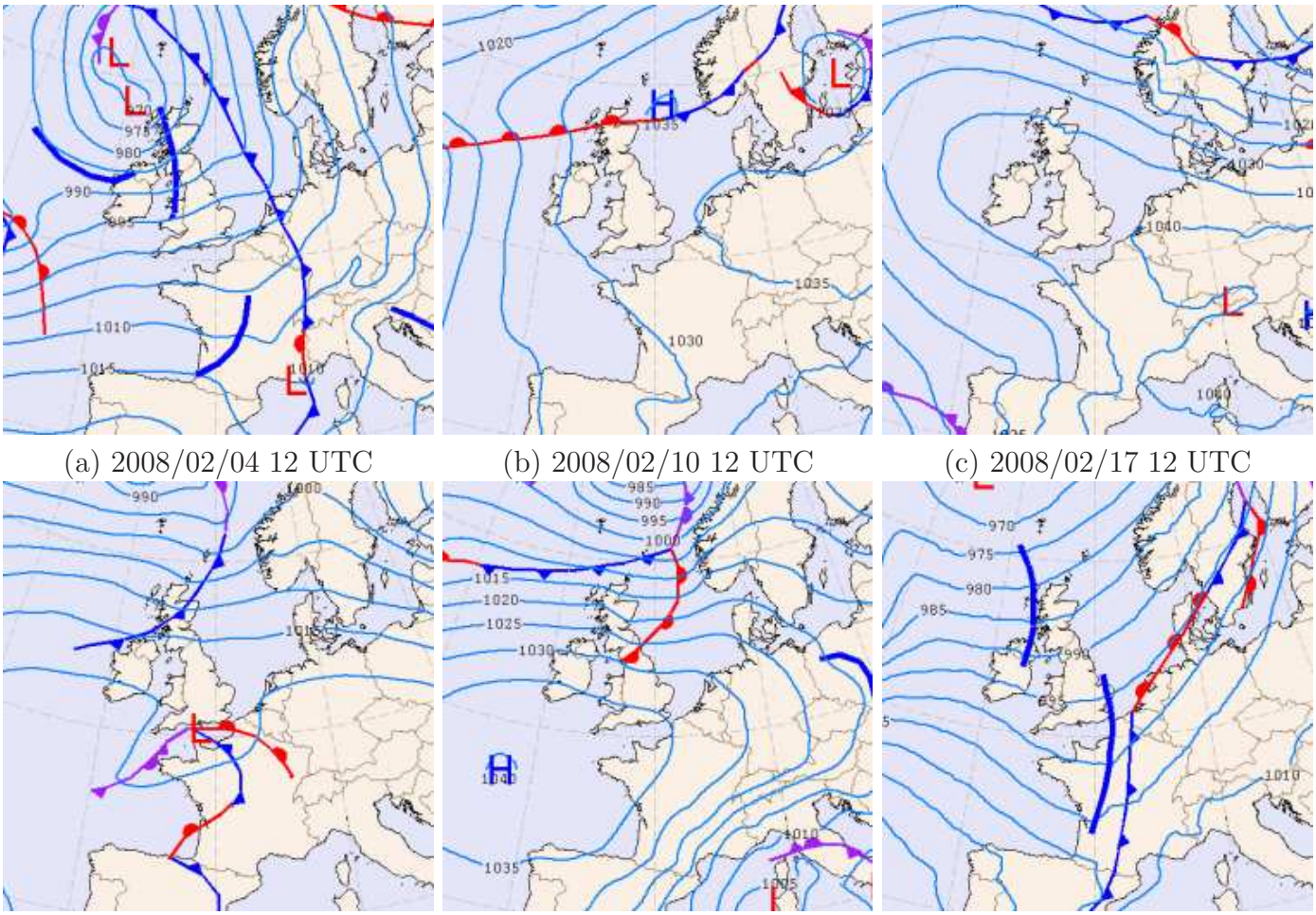

(a) 2008/02/04 12 UTC (b) 2008/02/10 12 UTC (c) 2008/02/17 12 UTC

(d) 2008/02/28 12 UTC (e) 2008/03/05 12 UTC (f) 2008/03/09 12 UTC

Figure 2.8: Synoptic weather analysis for the period 2008/02/01 to 2008/03/10.

displayed for the 4th Feb. 12 UTC. During these days the surface pressure gradually increases, while daily temperatures were between 1 and 10 degrees Celsius. This period of unsteady weather was followed by a high pressure ridge (see Fig. 2.8(b)) which resulted in a blocking high pressure system over the British Islands (see Fig. 2.8(c)). The surface temperature showed strong daily fluctuation.

Low pressure systems were able to pass the area around the Netherlands after the decay of the high pressure blockade (see Fig. 2.8(d)). The low pressure systems were followed by a high pressure region (see Fig. 2.8(e)), which was followed again by unsteady weather with some passing fronts.

The upper air wind clearly showed changes with the passing of the different weather systems. Periods of high winds are followed by low wind periods. Although the experiment period was a winter period, different wind regimes were present.

Additional information on the weather for some days can be found in Chapter 5 in which a number of selected cases are described.

# Chapter 3

# Numerical Weather Prediction

At KNMI a High Resolution Limited Area NWP Model (HIRLAM, Undén et al. (2002)) is run operationally for the short-term weather forecast. The version used in this study is HIRLAM 7.0, with additional KNMI adjustments. This version was operational from November 2006 upto mid January 2010. In January 2010 the operational HIRLAM version has been upgraded to HIRLAM 7.2.

The operational HIRLAM model has two cycles, one every six hours (called D11) with a forecast length of 48 hours, and one every three hours (called H11) with a forecast length of 24 hours. Both model-runs have horizontal grid of 11 kilometres; D11 has 60 vertical levels and H11 has 40 vertical levels, ranging from the surface to the top of the model atmosphere at 0.1 hPa. Assimilation of observations into NWP models is performed with the aim to find the best possible initial state of the atmosphere given the observations, an initial guess (also called background or first guess) and a priori defined constraints. From this initial state analysis a forecast can be computed through integration in time. Synoptic observations, such as wind, temperature and humidity from radiosonde and AMDAR and surface pressure observations, are used to constrain the initial state (the analysis) of the atmosphere with a state estimate of the previous model run (the so-called background). In case of the H11-cycle, a three-hour forecast of the previous H11-run is used as background information in the analysis. Because the model is a limited area model, the forecast at the boundaries of the region is equal to the forecasts from the larger HIRLAM D11-run (which has a six hour cycle). The latter six hour cycle is embedded in global forecast fields from the European Centre for Medium Range Weather Forecasting. Figure 3.1 shows the H11 and D11 NWP-regions.

The operational HIRLAM model run used non-separable background errors. For H11 we use an improved background error covariance description by Berre (2000) based on statistical balancing of wind, temperature and humidity. This will of course have an effect on the impact and we therefore did a reference run in the H11 domain, with ECMWF boundaries. The HIRLAM 3DVAR system is used. The settings of the reference run are copied in order to have a fair and realistic comparison of the forecasts with and without the new data. Note that the boundaries of the H11-run are different from the operational setting. However, because we are interested in the effect of new observations in the X11-domain on short forecasts (up to 5 hours) we expect that this influence is small.

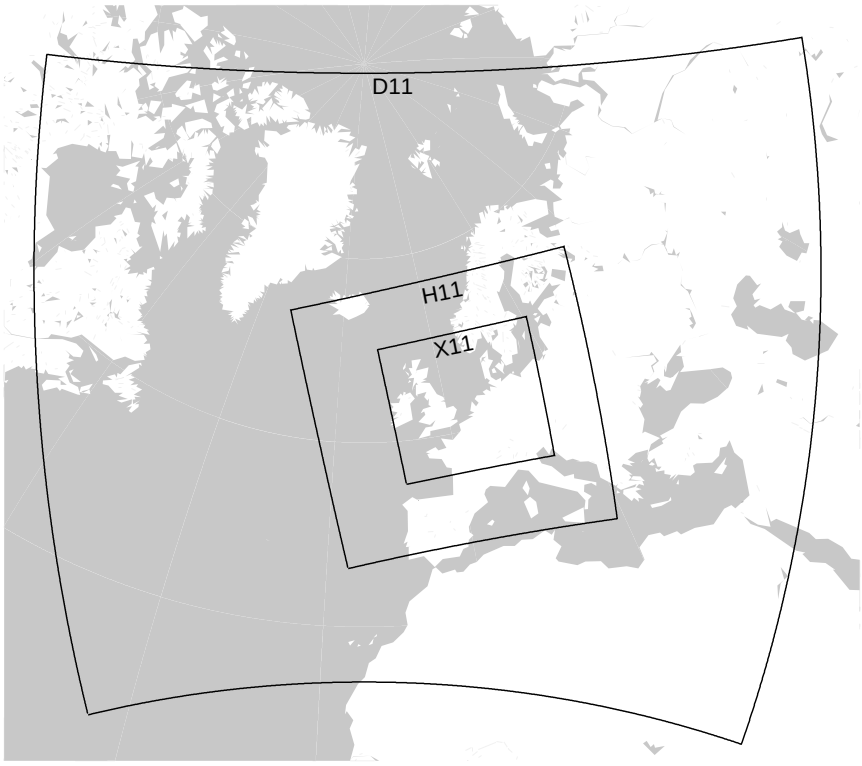


Figure 3.1: NWP model area of D11 and H11 and X11.

The NWP runs are performed on a region centered around the Netherlands and which includes the United Kingdom, Northern France the North Sea and Germany. Apart from the reference run, our experiments will be on a smaller domain, shown in Figure 3.1 by the smallest region called X11.

## 3.1 Boundaries

Limited area models are nested models and therefore need an external source which prescribes the model state at the boundaries. When integrated forward in time, this information will be advected into the model domain potentially causing detrimental interactions in the inner domain. The boundaries are generally available every three or six hours. During the forecast these boundaries are linearly interpolated in time to estimate the values at the boundaries. This linear interpolation introduces further errors at boundaries and thus forecast length should therefore be limited.

The experiments performed in this study are on region X11, which is small and therefore some notion on the effect of the boundaries should be gained. To investigate this effect we start with a reference run on the H11 domain and create a three hour forecast valid for 10 February 2008 03 UTC. A second run is performed based on the same analysis but on the smaller area X11. The boundaries for X11 are from the three-hour forecast of H11, that is at +00 and +03

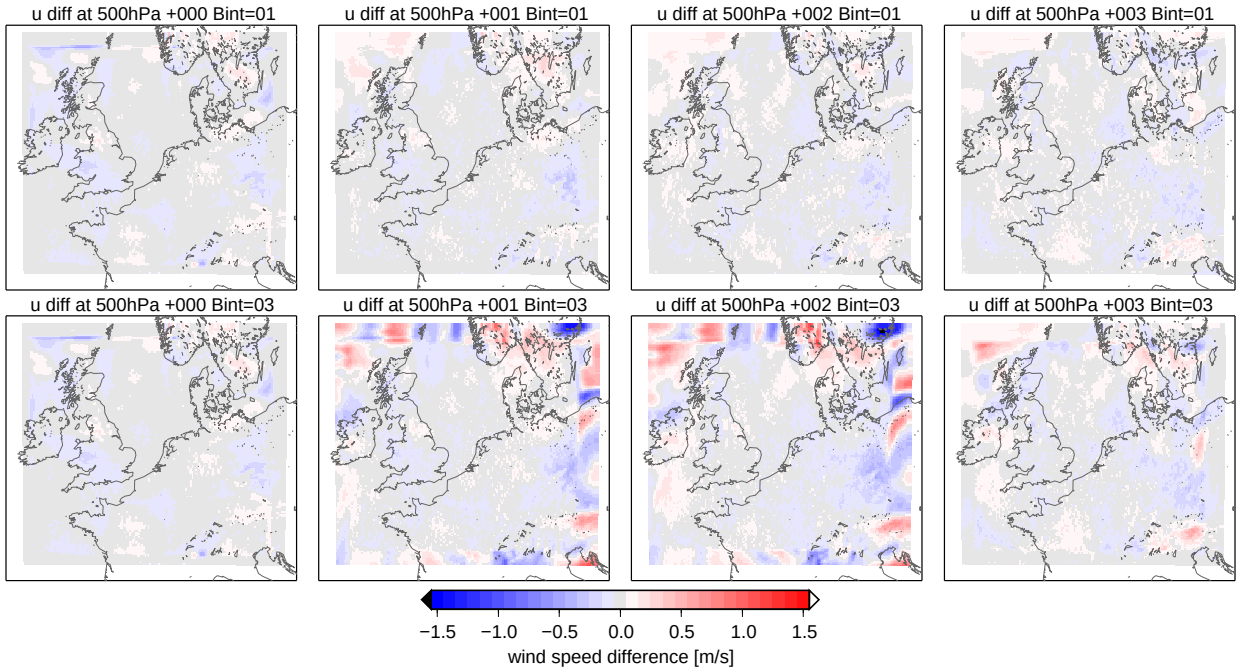


Figure 3.2: Difference in $u$-component of the wind at 500hPa between forecasts of H11 and two X11 runs started from the same analysis. The X11 run in the top row of panels uses hourly boundaries, while the bottom row has three-hourly boundaries. The forecasts are valid for 2008/02/10 03 UTC.

the boundaries are equal to the H11 +00 and +03 forecast, respectively. For reference, a third run, is performed which has hourly boundaries; this run is also on the X11 area.

In Figure 3.2 the difference between $u$-component wind forecast of H11 and X11 are shown for an X11 run with hourly boundaries (top row) and three-hourly boundaries (bottom-row). At analysis time (+000) the difference between H11 and X11 is numerical noise due to interpolation of the field. In the 1-hour forecast, effects near the lateral boundaries are clearly visible in the bottom row, while only small differences are observed for the run with hourly-boundaries (top row). The errors at the boundaries can be advected into the model domain, depending on the direction of the flow. North of Ireland, boundary errors at +001 are causing anomalies at later forecast times. This disturbance is clearly less when hourly boundaries are used. Figure 3.3 shows the difference in $u$-wind forecast between the two hourly runs at +003. The anomalies near the boundaries are clearly visible.

In this study we will use hourly boundaries to diminish the boundary effect for NWP-runs performed on the X11 domain. Nevertheless, errors will introduce flow discrepancies in X11 and H11 at the boundaries and thus the forecast length is limited to maximum 4 hours. This can be regarded as a conservative choice.

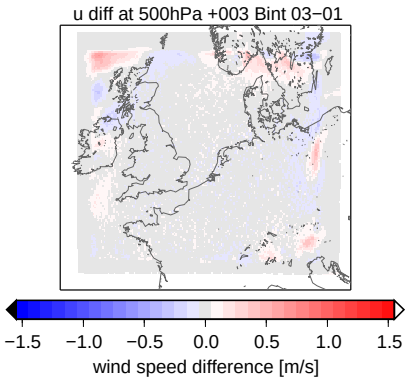


Figure 3.3: Difference between the three-hour forecasts of the hourly runs at 500hPa for $u$-component of the wind.

## 3.2 Experiments

In Table 3.1 the five different experiments are described. Two experiments have a three-hour cycle, while the other three have a hourly cycle. The boundaries used in the three-hourly cycles (REF and REF+M) are obtained from the operational ECWMF run, while the boundaries of the hourly runs are forecast fields of (at most) a three-hour forecast from the REF-run. Because the domain on which the hourly experiments are performed is small (the X11-region, see Fig. 3.1) these runs have hourly boundaries to reduce the interpolation effects at the boundaries.

The hourly runs can be run in near real-time, because the Mode-S data are available within (at most) 10 minutes after observation time. This fast delivery of the observations opens the possibility to apply the NWP model for now-casting purposes.

The main difference between the experiments is, apart from the domain and cycling period, the type and amount of observations used.

Table 3.1: Experiments description.

| Abbreviation | Description | Cycle (hr) | Boundary source | Boundary Interval (hr) | Domain | Observation cut-off time (min) |
|---|---|---|---|---|---|---|
| REF | Reference run | 3 | ECMWF | 3 | H11 | 60 |
| REF+M | Assimilation of standard observations + Mode-S | 3 | ECMWF | 3 | H11 | 60 |
| A-01 | Assimilation of rapid available observations (AMDAR+synop) | 1 | REF | 1 | X11 | 10 |
| M-01 | Assimilation of Mode-S and rapid synop observations | 1 | REF | 1 | X11 | 10 |
| M+A-01 | Assimilation of Mode-S and rapid available observations (AMDAR+synop) | 1 | REF | 1 | X11 | 10 |

# Chapter 4

# Assimilation Impact Results

## 4.1 Comparison against Mode-S

In this section, Mode-S observations are compared to the forecast fields of all the experiments. The Mode-S observations are calibrated and corrected as described by De Haan (2009) at the full hour and the half hour. Observations plus and minus 10 minutes around the validation time are used for the comparison. For the half hour comparisons, a linear interpolation in time of the forecast fields is applied. In figure 4.1 the results are shown for the forecasts from zero (i.e the analysis) to four hours ahead. The statistics only show data from runs started at 00, 03, 06, 09, 12, 15, 18 and 21 UTC to have a one-to-one comparison between the different experiments.

The first observation from Figure 4.1 is that the experiment with only AMDAR observations has the worst RMS for both temperature and wind. Furthermore, with increasing forecast length all RMS are converging.

Obviously at analysis time, all experiments using Mode-S observations show the lowest bias and RMS for temperature, wind speed and direction. The bias shows no jump during the first hour, indicating consistency between model and observation. For all experiments using Mode-S data, it turns out that after a few hours the RMS converges to the RMS of the REF-run, except for wind speed for the M-01 run where the RMS becomes slightly larger.

The positive impact on temperature RMS has disappeared after 90 minutes at 875hPa and 225hPa, and after 30 minutes at 400hPa and 600hPa.

For wind speed RMS, the positive improvement on RMS stays longer in the forecast (i.e. 3 hours at 850hPa, 2 hours at 600hPa and 225hPa and 90 minutes at 400hPa). The wind direction RMS displays a longer positive impact (3 to 4 hours depending on the level). The strong increase in RMS in the first 30 minutes at 400hPa and 225hPa is remarkable and is not present in the lowest level. This strong increase in RMS in the first half hour is also observed for wind speed at the top two levels and temperature at the top three levels. For a single observation with estimated random error equal to the estimated background error, the analysis error will be a factor of 0.7 of the background error. So the observation minus model RMS differences are on this basis expected to rise by 15% from the analysis (+000) to the first guess (+001). This is in line with the plots.

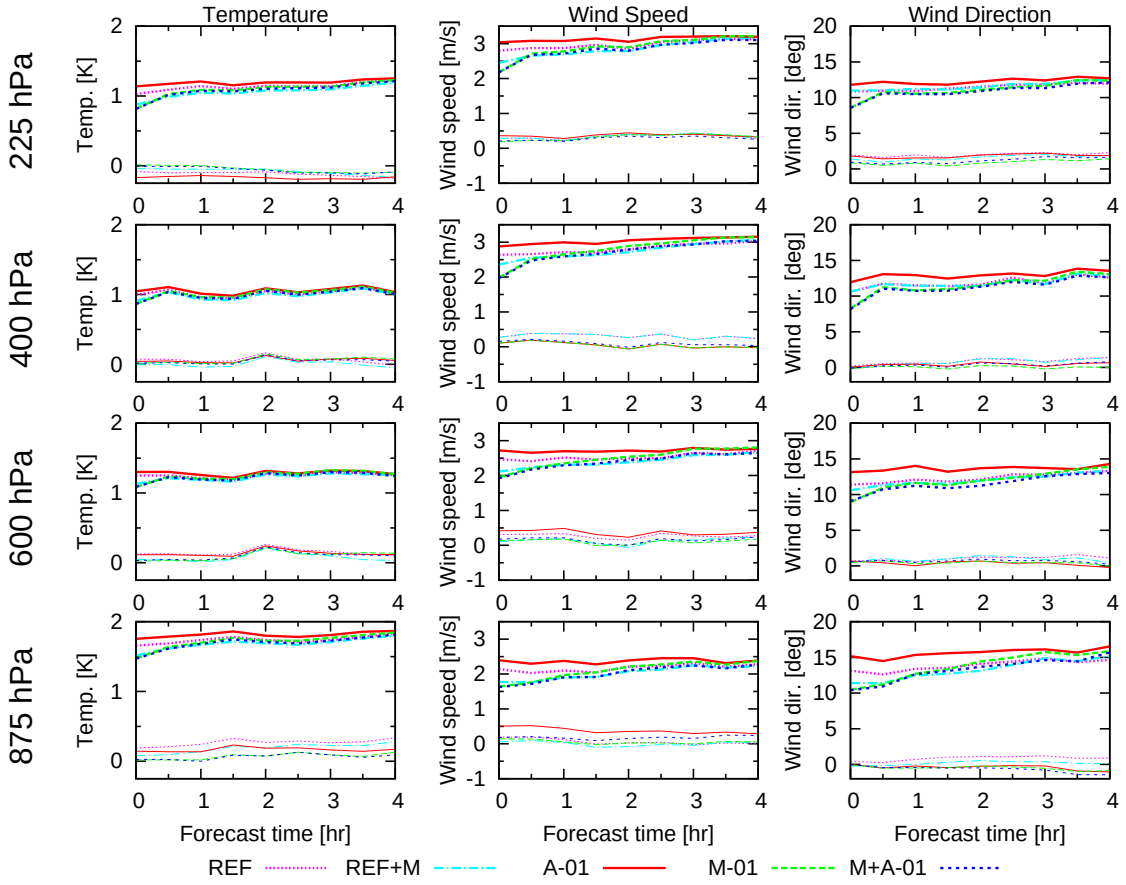


Figure 4.1: Statistics of the comparison of the model forecasts against Mode-S observations at the full and half hour. Thick lines represent the RMS; the thin lines (lowest values) denote the bias between model and observation.

The bias also shows a positive impact for experiments with Mode-S-observations, especially at the lowest levels; for wind speed a positive impact on the bias is observed at all levels (however less at 875hPa when compared to the other levels).

The impact of Mode-S observations on temperature is almost neutral. For wind (speed and direction) there are some small differences between the experiments that use Mode-S-observations. REF+M is at analysis time worse than all the other Mode-S-experiments. This might be due to the difference in cycling period, resulting in smaller analysis increments for the X11 domain. A positive impact on wind direction RMS and bias for REF+M is only observed at 875hPa. At higher levels no positive impact is observed. For wind speed, REF+M shows similar forecast impact as M+A-01.

Apart from 875hPa, the wind speed bias of the Mode-S experiments are equal or better than REF. At 875hPa, M+A-01 has the smallest and most constant bias.

For temperature, all biases are almost equal, except again for 875hPa, where the two hourly experiments show a smaller bias. Wind direction biases show similar statistics. The experiment

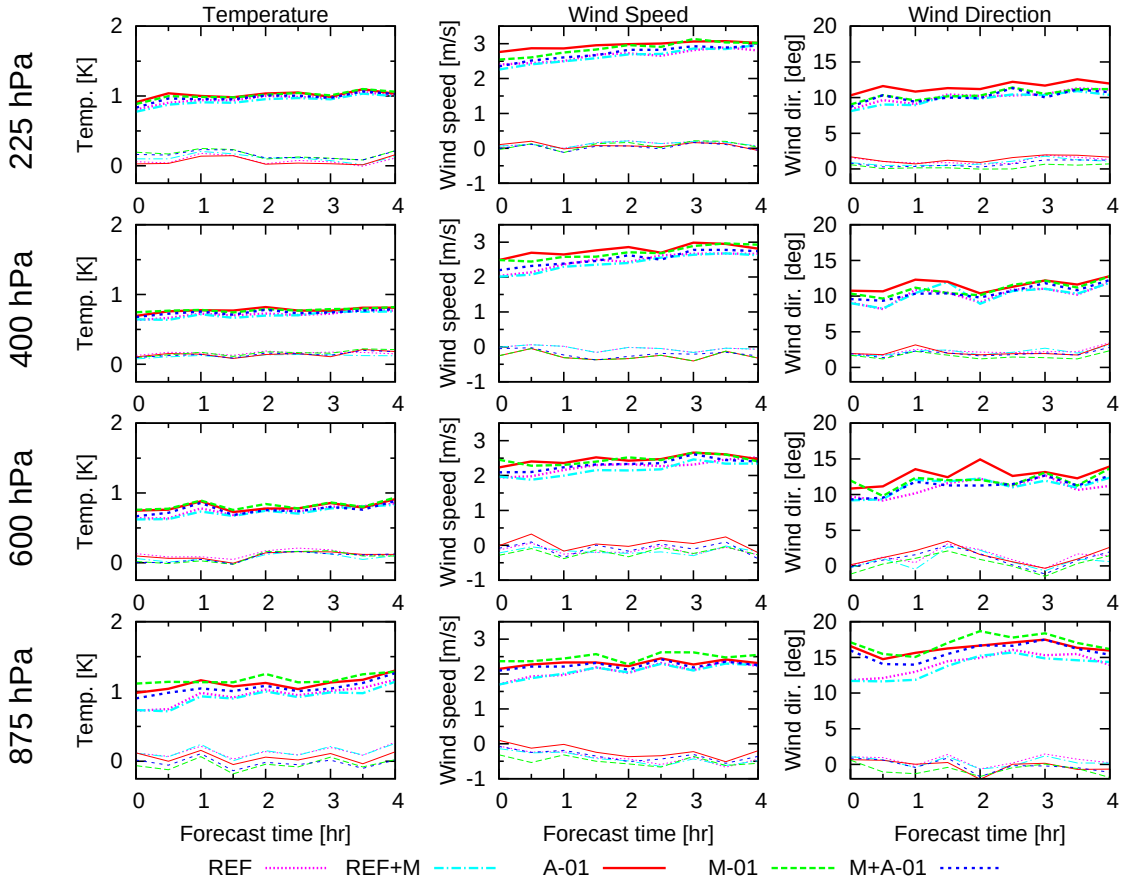


Figure 4.2: Statistics of the comparison of the model forecasts against AMDAR observations at the full and half hour. Thick lines represent the RMS; the thin lines (lowest values) denote the bias between model and observation.

A-01 is worts in all parameters and at all levels. This could be due to short cut-off time of the observations.

qOverall, in the lowest level both hourly cycles using Mode-S observations show a positive impact (bias and RMS). The hourly run with only AMDAR observations shows a clear negative impact. At higher levels a positive impact is observed for RMS, however this impact disappears after a certain forecast length, where the duration of the positive impact differs for different levels and parameters. Experiment M-01 has a negative impact after 2 hours (for temperature and wind speed RMS). Adding information from AMDAR (mainly from surrounding airports) improves the impact also for longer forecasts.

## 4.2 Comparison with AMDAR Observations

In this section, AMDAR observations are used to assess the quality of the forercasts of the different model runs. These AMDAR observations are obtained through the GTS and are

screened for gross errors, such as zero wind speed and wind direction. This happened for a number of specific aircraft, and these are excluded from the data set. Moreover, using a visual check on outliers in wind speed and direction in the lowest level is performed and these outliers are also excluded from the dataset.

Not all AMDAR observations used in the comparison are actually assimilated due to the time of presence with respect to the observation cut-off time of a model run. For instance, the three-hourly REF-runs have a cut-off time of +1 hour, while all the hourly runs have a cut-off time of +10 minutes (relative to the assimilation time).

Figure 4.2 shows the bias and RMS for temperature, wind speed and wind direction for four levels. The RMS for temperature is clearly lower for all levels and models when compared to the RMS for temperature shown in Figure 4.1. This is in line with the results found in De Haan (2009): Mode-S temperature observations are of lower quality than the AMDAR temperature observations. For temperature, the benefit of assimilating AMDAR is most visible at the lowest levels in the first two hours of the forecast.

For wind speed we see a similar effect. The REF-runs perform better in the lowest levels up to 2 hours in the forecast; after 2 hours no significant difference can be observed. The wind direction has worse statistics, especially in the lowest level. Figure 4.2 shows that A-01 has the worst wind statistics, while the three-hourly runs (REF and REF+M) have the best statistics in the first hours of the forecast. Apart from the lowest level, the run M+A-01 has the best statistics of the hourly runs with equal quality to the three-hour runs after 2 hours in forecast time.

Note that the wind statistics at the lowest level are puzzling. Because of the low amount of observations used in the comparison (around 1000 for AMDAR at 875hPa over a six week period) it might still be that some undiscovered outliers influence the statistics. Remarkable is the decrease in wind direction RMS at 875hPa for a forecast time of 4 hours for all model runs, while a local maximum in RMS occurs at around 2 to 3 hours in the forecast.

## 4.3 Comparison with Radiosonde Observations

In this section, radiosonde observations obtained at De Bilt are used to evaluate the forecasts of the different experiments. The full (10 second) resolution radiosonde observations are used for the comparison. The full resolution wind and temperature observations are not assimilated but a subset (i.e. 50 so-called significant levels) of these full profiles instead. So, at $t = 0$ hour some dependency of the analysis on the verification data may exist, most strongly in REF since few other observation sources are used.

Because the REF and REF+M run have a three hour cycle and the radiosonde are launched only two times a day it is only possible to compare radiosonde observations at analysis time and at a three hour forecast. For the other experiments, a comparison can be made with other forecasts lengths. Note that due to the lack of data around +01 UTC the forecast from the hourly-cycles with Mode-S data assimilated could be of less quality. This fact will not show up in the comparison because only forecasts started at 08, 09, 10, 11, 12 and 20, 21, 22, 23 and 00 UTC are used in the comparison. At these times Mode-S observations are available and are

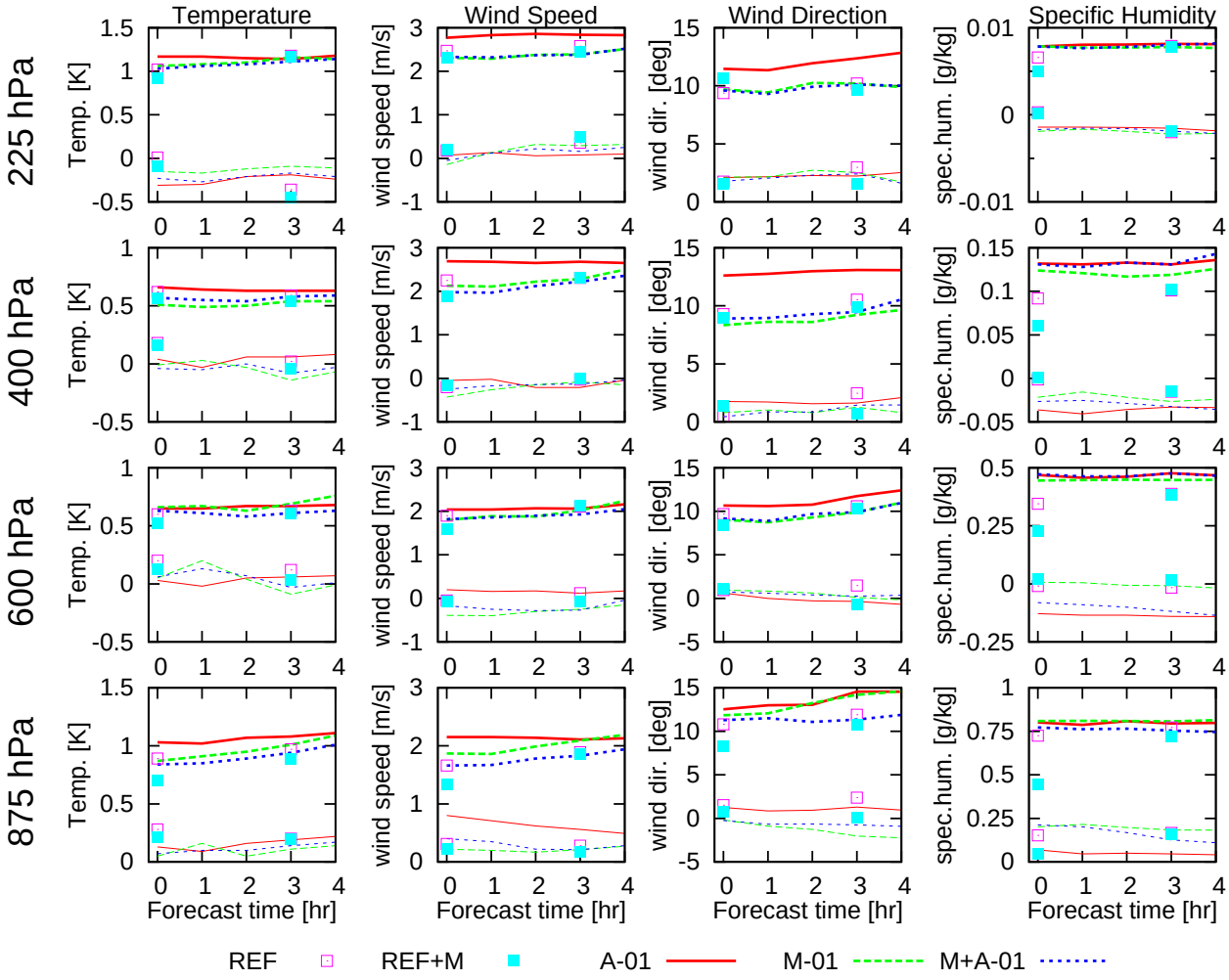


Figure 4.3: Statistics of the comparison of the model forecasts against radiosonde observation from De Bilt. Thick lines represent the RMS; the thin lines (lowest values) denote the bias between model and observation.

thus assimilated into the REF+M, M-01 and M+A-01 runs.

In Figure 4.3 the statistics of the experiments for four levels are shown. Again, the A-01 runs shows the worst RMS-statistics generally. For temperature and wind speed the RMS converges, however, where for wind direction a difference of 1 to 2 degrees in RMS is observed for the whole profile and all forecasts.

For almost all levels at analysis time (+00) the temperature RMS for the REF and REF+M runs is smaller than the M-01 and M+A-01 runs; the exception is level 400hPa. This should be the case because these observation are assimilated in these runs. The bias, however, is smaller for the hourly runs (except 225hPa). Furthermore, the bias for M+A-01 is more constant over the forecast window than M-01, but the difference is not very large. At +03 the temperature RMS of M+A-01 is close to the RMS of the three hourly runs, with REF+M being the smallest

on all levels, although the difference at levels higher that the bottom level is very small. Apart from the 400hPa level, the M+A-01 run has a smaller RMS over the whole forecast window.

The statistics for wind speed show a clear impact of Mode-S at the lowest level. At analysis time the three-hour runs have the smallest wind speed RMS at all levels. In the top three levels the hourly runs have a smaller wind speed RMS at +03 than the three-hourly runs. There is no significant difference between M-01 and M+A-01 at these levels. In the bottom level M+A-01 has the smallest RMS over the whole period (including +03). The wind speed biases differ for the lowest levels. A-01 has a positive bias, while the other biases are close to zero. The M+A-01 runs shows to have the smallest bias, apart from the first hours at the 875hPa level.

For wind direction, the differences between M-01 and M+A-01 are small at the top three levels for both bias and RMS over the whole forecast window. At analysis time, the REF+M clearly shows the smallest RMS for the lowest levels. The biases are close except in the lowest level, where the hourly runs have the smallest bias. At this level the RMS of M+A-01 is clearly better and more constant than M-01. At +03 REF+M and M+A-01 are close, while REF and M-01 have much larger wind direction RMS's.

For specific humidity, no (large) impact for the hourly runs is expected because no humidity information is assimilated in these runs. A relation between humidity and temperature exists, so by changing the temperature, humidity fields are also adjusted. The figure shows constant RMS for the hourly runs at all levels, with REF+M being the smallest. Note the difference between REF and REF+M at analysis time; both bias and RMS are better for REF+M than for the REF run.

In conclusion, the largest impact on wind speed and direction RMS was observed in the lowest levels with experiment M+A-01. The A-01 experiment shows a negative impact in temperature, wind speed and direction. The REF analysis dependency on the radiosonde profile is visible in Figure 4.3. It is remarkable that REF+M compares better to radiosondes at $t = 0$ than REF. This indicates that a large consistency of the Mode-S observations and radiosonde observations exists.

## 4.4 Observation minus Background and Analysis

The Mode-S observation minus background bias and RMS are shown in Figure 4.4 for the two hourly runs which assimilate Mode-S observations. The bias and RMS in the $u$-component of the wind is reduced when additional AMDAR observations are introduced in the assimilation. The RMS in the $v$-component also decreases; the bias shows a mixed impact. For temperature no significant improvements are observed.

When the analysis statistics of the Mode-S observations are inspected (see Fig. 4.5) one can see that there are small improvements in wind RMS. Again, the bias in $u$-component is better with additional AMDAR observations and a mixed impact on the $v$-component is observed. As before, no significant impact on temperature is noted.

To obtain some notion on the relative weight of the background we compare background errors with analysis errors and assume

$$< o - b >^2 = \sigma_o^2 + \sigma_b^2, \tag{4.1}$$

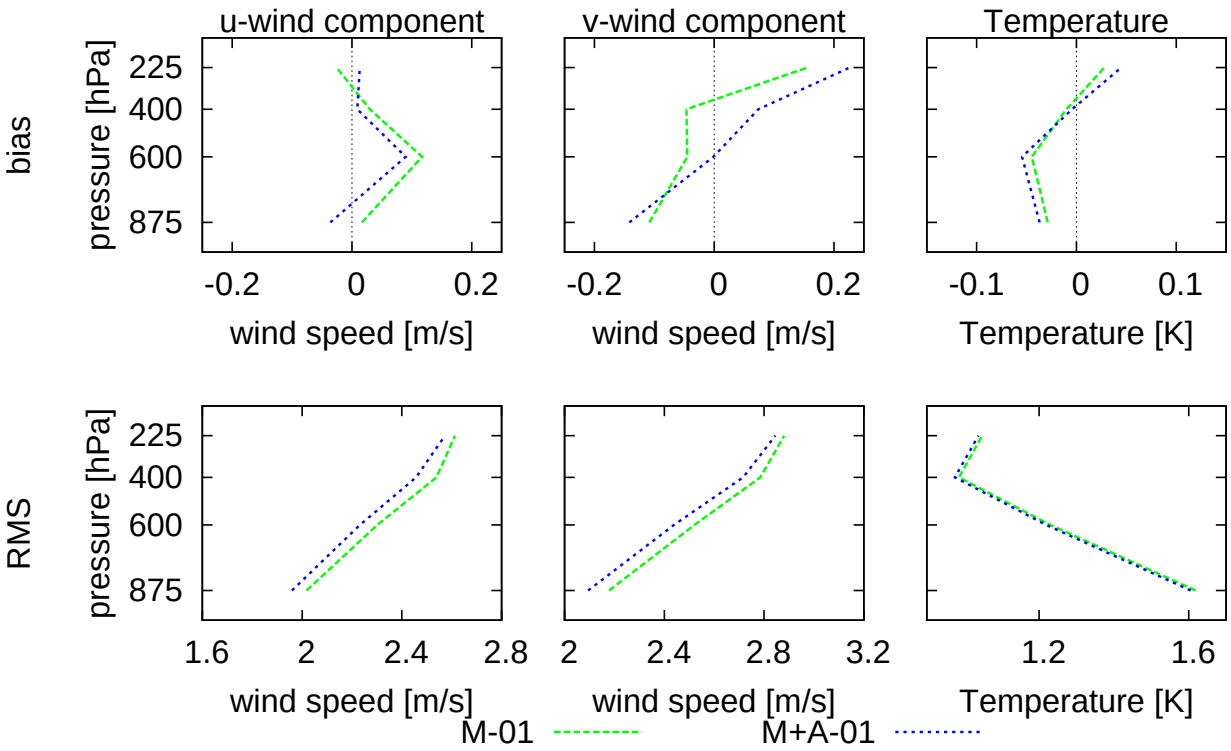


Figure 4.4: Observation minus background statistics for Mode-S observations

where "<>" represents the mean. Further, when we assume equal observation and background errors ($\sigma$) in M-01 then

$$\sqrt{< o - b >^2} = \sqrt{2}\sigma. \tag{4.2}$$

When assimilating a single observation we expect that

$$\frac{1}{\sigma_a^2} = \frac{1}{\sigma_o^2} + \frac{1}{\sigma_b^2} \tag{4.3}$$

and thus

$$\sqrt{< o - a >^2} = \sqrt{\sigma_o^2 + \sigma_a^2} = \sqrt{\sigma^2 + \sigma^2/2} = \sqrt{3/2}\sigma, \tag{4.4}$$

which is a factor of 0.87 lower than the o-b. Looking at the plots, Mode-S impact appears slightly larger. Nevertheless, when $\sqrt{< o - b >^2}$ improves in M+A-01 by 10% with respect to M-01, it indicates an improved background error by 20%. This would lead in this hypothetical case to an improvement in the analysis of 6% and a reduction of $\sqrt{< o - a >^2}$ of 2%. Similarly, for a background error of $2\sigma$, that is twice the observation error the 10% improvement in $\sqrt{< o - b >^2}$ would improve $o - a$ by only 2.5%. This appears similar to our results, indicating a relative large weight of the observations due to their density and at the same time a beneficial forecast impact.

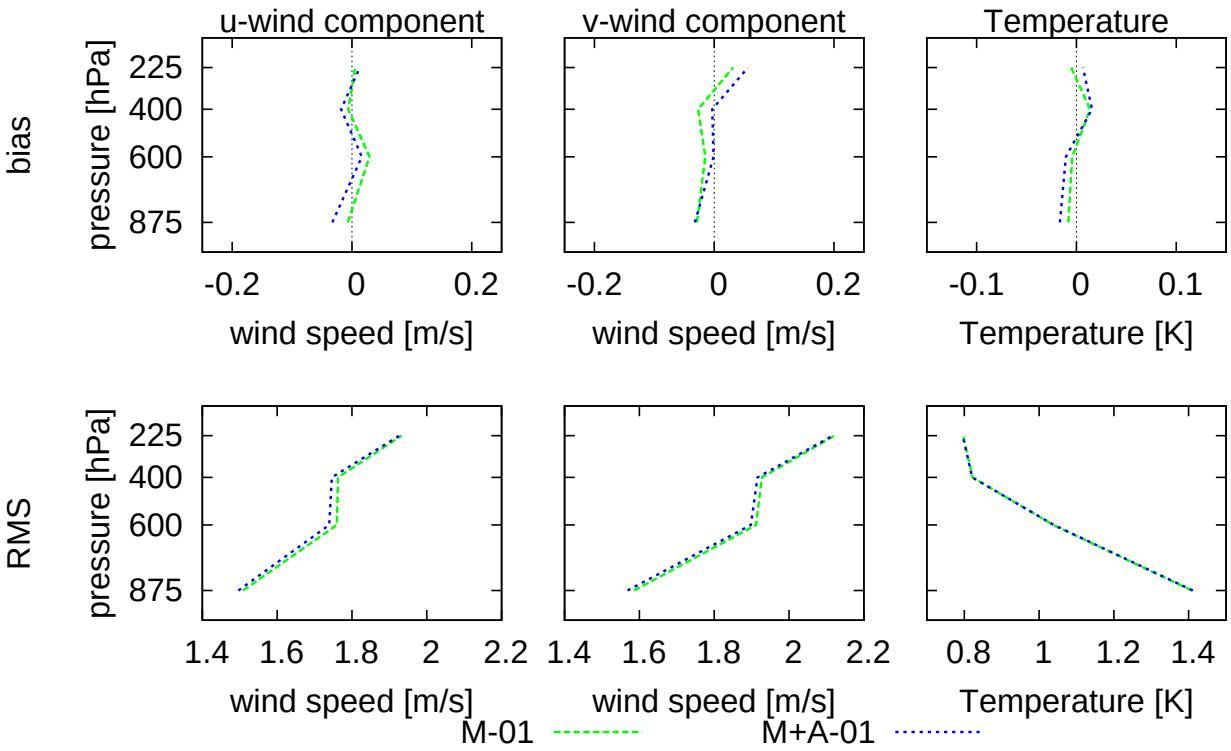


Figure 4.5: Observation minus analysis statistics for Mode-S observations

## 4.5 Nowcasting quality

In the previous sections we showed that assimilating Mode-S data in an hourly cycle has a positive impact on wind and temperature forecasts, when compared to Mode-S observations and radiosonde observations. However, after a few hours this positive impact has disappeared.

For operational purposes that require a very short timeliness, the quality of the forecast in "real-time" is essential. "Real-time" applications include now-casting (forecast ranges up to a few hours) or supplying meteorological information for air traffic control to guide continuous descent approaches of aircraft. These real-time applications will benefit from rapid updates of a numerical weather prediction model when Mode-S observations are assimilated and the update frequency is one hour. Using an hourly cycle, the forecast length used for now-casting applications will be between one and two hours, while for a three-hourly cycle the forecasts lengths will be between two and five hours. On the other hand, more analyses have to be run and some types of observations arrive too late to be included in the assimilation (e.g. radiosondes, some satellite data).

In Figure 4.6 the statistics of experiments REF, M-01 and M+A-01 are shown when compared to Mode-S observations in "real-time". In line with above results, the best statistics are obtained when both Mode-S and AMDAR are assimilated.

The largest profit is gained when the assimilation frequency is increased from once per three hours to once per hour. A small additional improvement is found when AMDAR information is

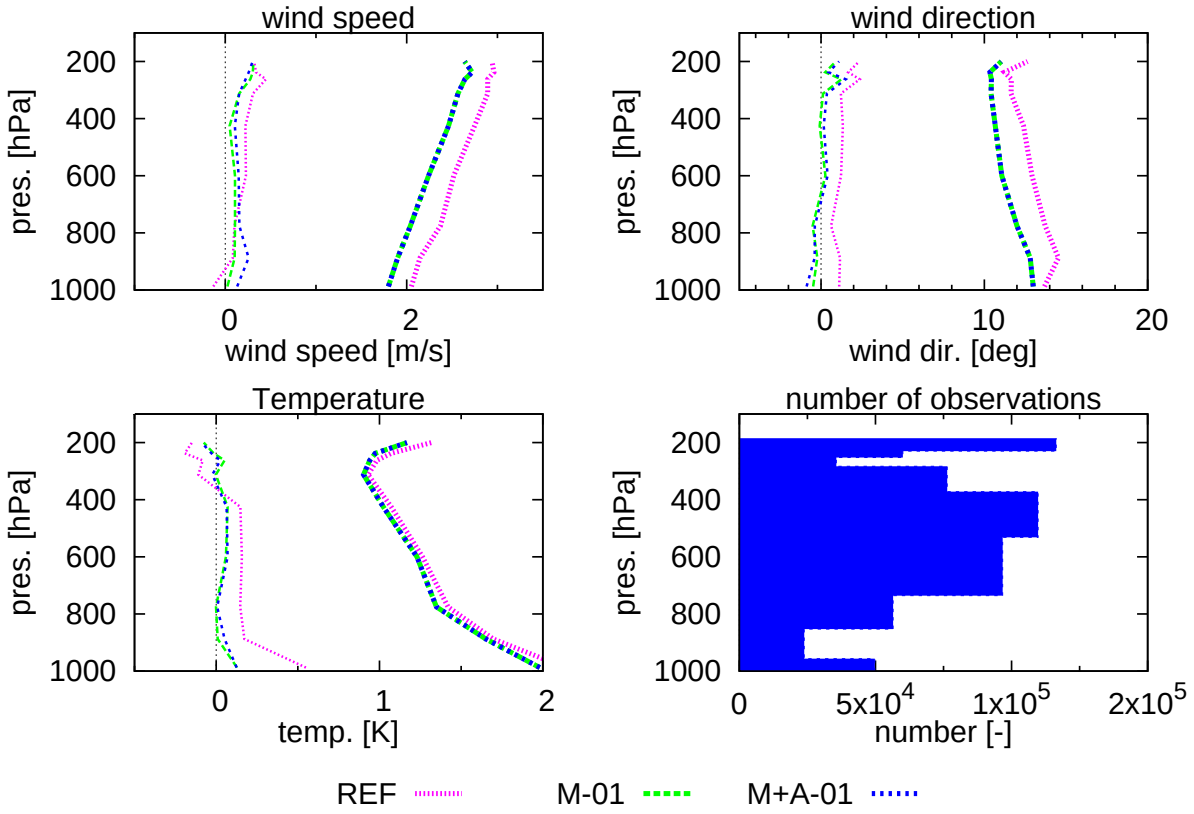


Figure 4.6: "Real-time" comparison of the different forecasts against Mode-S observations. For REF the forecast length is minimal 2 hours, while for M-01 and M+A-01 it is maximal 2 hours.

assimilated as well. As stated before, adding AMDAR will improve the forecast over the whole forecast range, with the emphasis on +02 to +04, when compared to the hourly run without AMDAR.

# Chapter 5

# Results for Selected Cases

A number of cases have been selected which display differences between the REF-run and the M+A-01-run. The selection criteria for the cases were 1) large difference in wind speed with either observations or between the models, 2) large offsets of the Mode-S observations with the background, and 3) additional wind observations from dual-doppler radar were present. Criteria 1) and 2) draw the attention to cases where the atmospheric condition is uncertain and/or where Mode-S has large impact; either benificial or detrimental. With criterion 3) these cases may be tetsted against independent observations to verify whether Mode-S brings improvement or not.

The dual-doppler wind observations are obtained from observed doppler shift when the radar signal is reflected by droplets. When a droplet is illuminated by two radars it is possible to estimate the velocity vector of the droplet. The mean velocity in the field of view is highly correlated with the wind. There are of course limitation to this method, being the radar ambiguity velocity, geometric restriction by the radar locations. The fact that an overlap is needed to calculate a wind vector from the doppler velocity limits the horizontal coverage, as is shown in Figure 5.1. A report on the quality of these wind observation is in preparation.

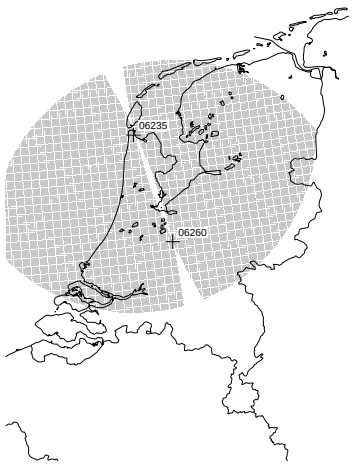


Figure 5.1: Coverage of the DUAL-radar vector wind observation.

## 5.1 20 February 2008: 00 - 06 UTC

A westerly flow transported warm air towards the Netherlands. Low pressure systems moved from the North Atlantic to Scandinavia, while over Southern Europe a high pressure system was situated. On February 20, 2008 a weak trough moved over the Netherlands. See Figure 5.2.

On 20 February 2008 00 UTC, Figure 5.3 shows large differences in the north-west of the region both at the 700hPa and 925hPa level. The wind direction is clearly more from the west in the REF-run. There are no (Mode-S) observations to support this direction of the flow. For locations where there are observations, the M+A-01-run is more in-line with these observations (see Figure 5.3 top panels). A cross-section, along the line displayed in the top panels of Figure 5.3 shows a strong wind shear in the boundary layer. Differences in wind direction between 700hPa and 500 hPa. M+A-01 and REF both match the radiosonde report from 900hPa onwards (see Figure 5.3 bottom panel).

Figure 5.4 shows the horizontal wind fields at 03 UTC. Note that no Mode-S, AMDAR or radiosonde observations were present. Again a large difference in wind direction between the two runs in the top part of the picture. The strong wind shear in the boundary layer, as observed at 00 UTC, is still present. The M+A-01-run matches the radar winds better (see Figure 5.4).

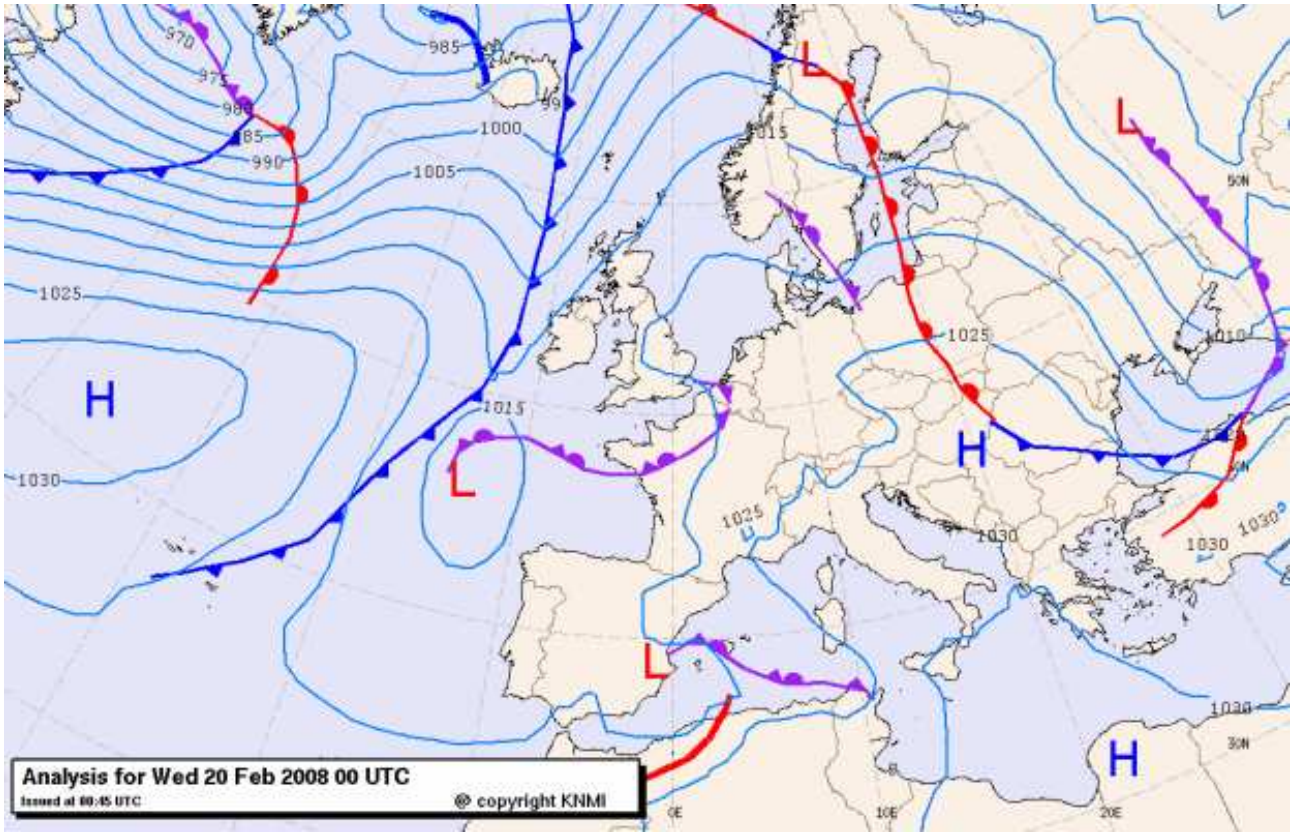


Figure 5.2: Analysis from KNMI based on HIRLAM analysis of February 20, 2008 00 UTC.

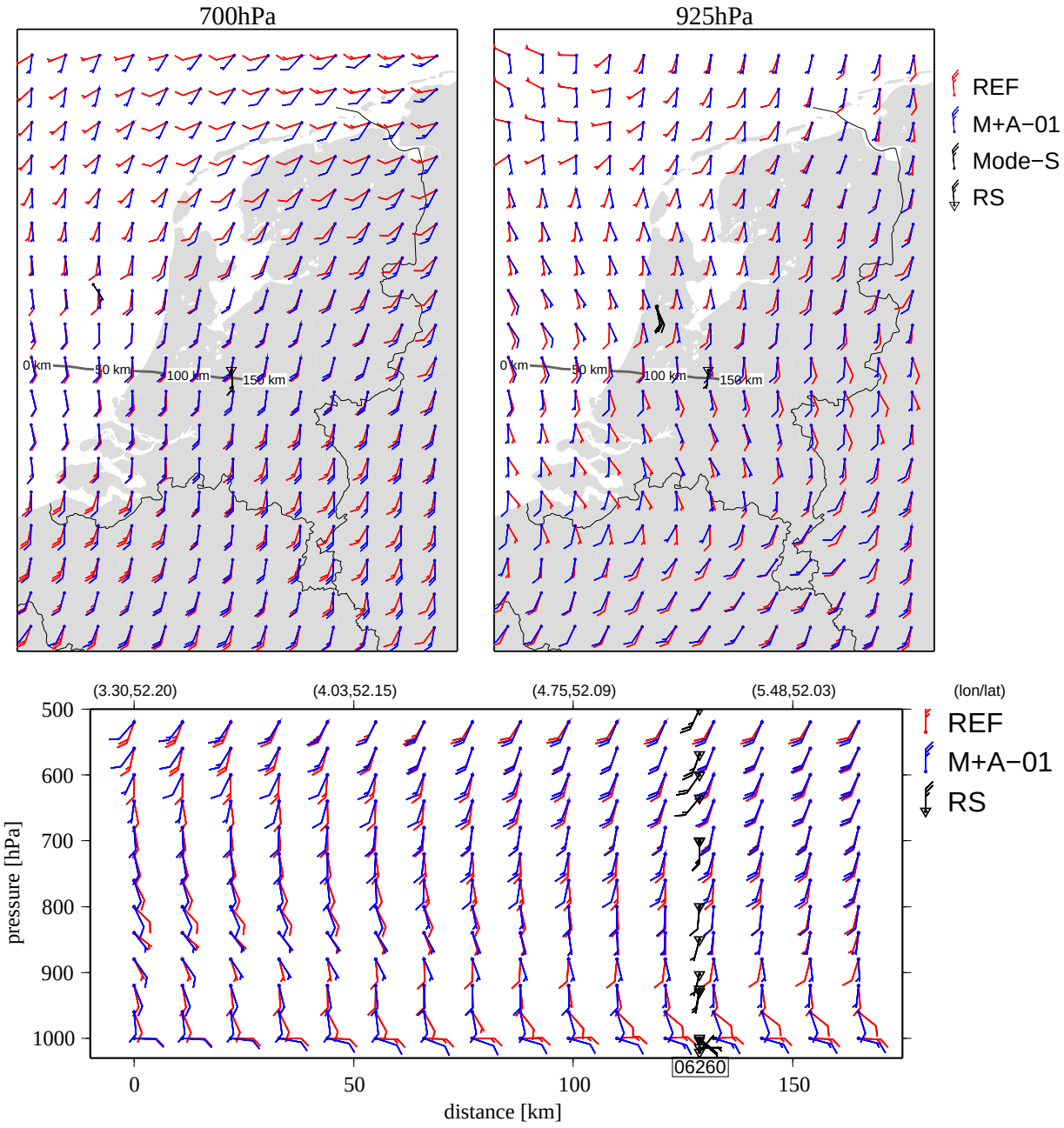


Figure 5.3: Top panel: wind barbs for two experiments together with radiosonde wind observations; the REF-run (red) and the M+A-01-run (blue). Bottom panel: vertical cross-section along the line displayed in the top panel. Inverse triangles denote the radiosonde De Bilt observations. . The plotted fields are the analyses valid for 20 February 2008, 00 UTC.

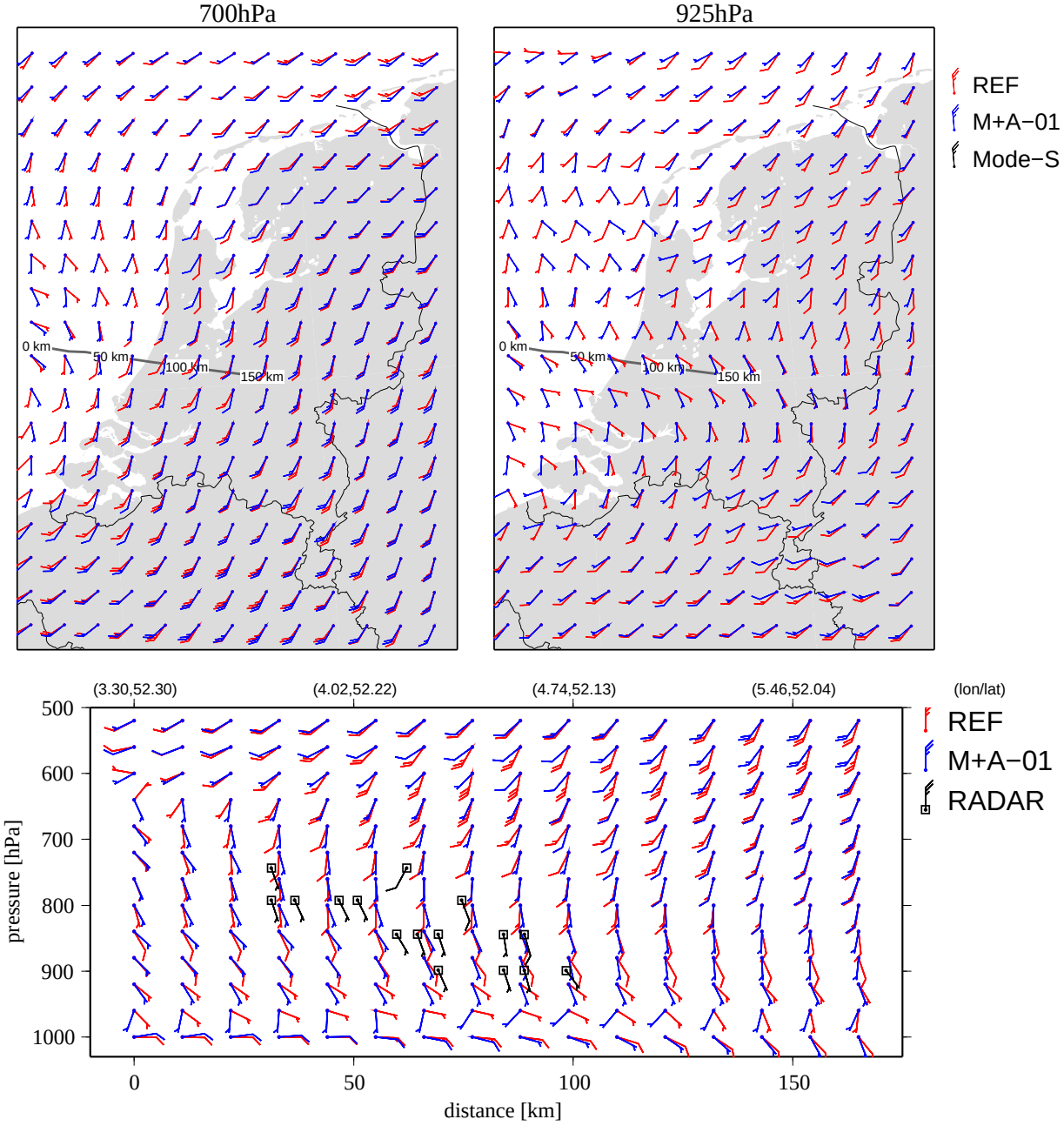


Figure 5.4: Wind fields for the REF-run (red) and M+A-01-run (blue) valid on 20 February 03 UTC. The squares denote the dual-radar wind observations at 1, 1.5, 2, and 2.5 km.

On 20 February 2008 06 UTC horizontally small scale structures are observed by the model runs. Unfortunately, these small structures can not be verified by upper air wind observations from aircraft (see Figure 5.5). The vertical cross-section shows that model runs do not match

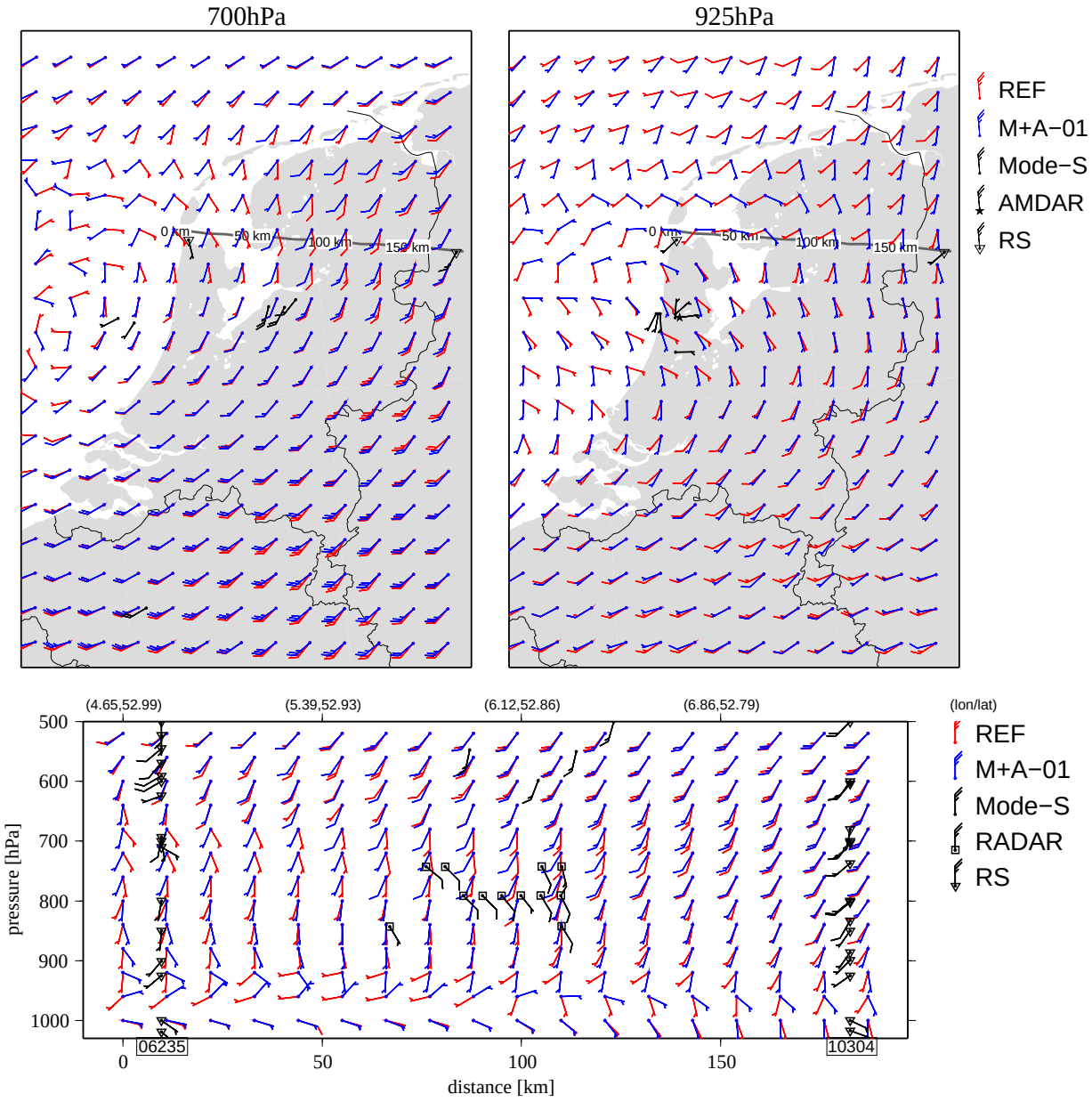


Figure 5.5: Wind fields for the REF- and M+A-01-run valid on 20 February 06 UTC. The squares denote the dual-radar wind observations at 1, 1.5, 2, and 2.5 km. In black are Mode-S observations and the inverse triangles are radiosonde observations from 06235 and 10304.

the radar observations. It is suspected that the radar observations are wrong, because the wind field matches the radiosonde and Mode-S observations, and the deviation between radar and both models is large. Note that there is some signal of a more easterly wind in the radiosonde observations 06235 just below 700 hPa. This wind vector is not observed in the two model runs. The M+A-01 run from 900hPa onwards matches the radiosonde (06235) better than the

REF-run. Note that the vertical cross-section has been shifted to the north with respect to the previous figure, to capture the radiosonde observations (see Figure 5.5). In the lowest level both models do not match the radiosonde observation from 10304. This may be due to shallow structure functions which tends to spread information over a too large area.

In summary, The M+A-01 run is more in line with the observations than REF, while for areas with large differences in wind velocity no assessment of quality can be made.

## 5.2 24 February 21 UTC - 25 February 00 UTC

A cold front passed the Netherlands during the night of 24 February to 25 February (see Figure 5.6). On the Dutch Wadden-islands (in the north) 10mm of precipitation was observed. Figure 5.6 shows the analysis at 25 February 00 UTC. The wind speeds accompanying the cold front were moderate, as can be seen from the pressure pattern. At 24 February 21 UTC, before the cold front the winds at 925hPa and 700hPa were generally from west to south-west (See Figure 5.7, top panels).

The REF-run shows more wind direction variability than the M+A-01-run. The latter run matches the Mode-S observations better at 925hPa. The bottom panel in Figure 5.7 shows the

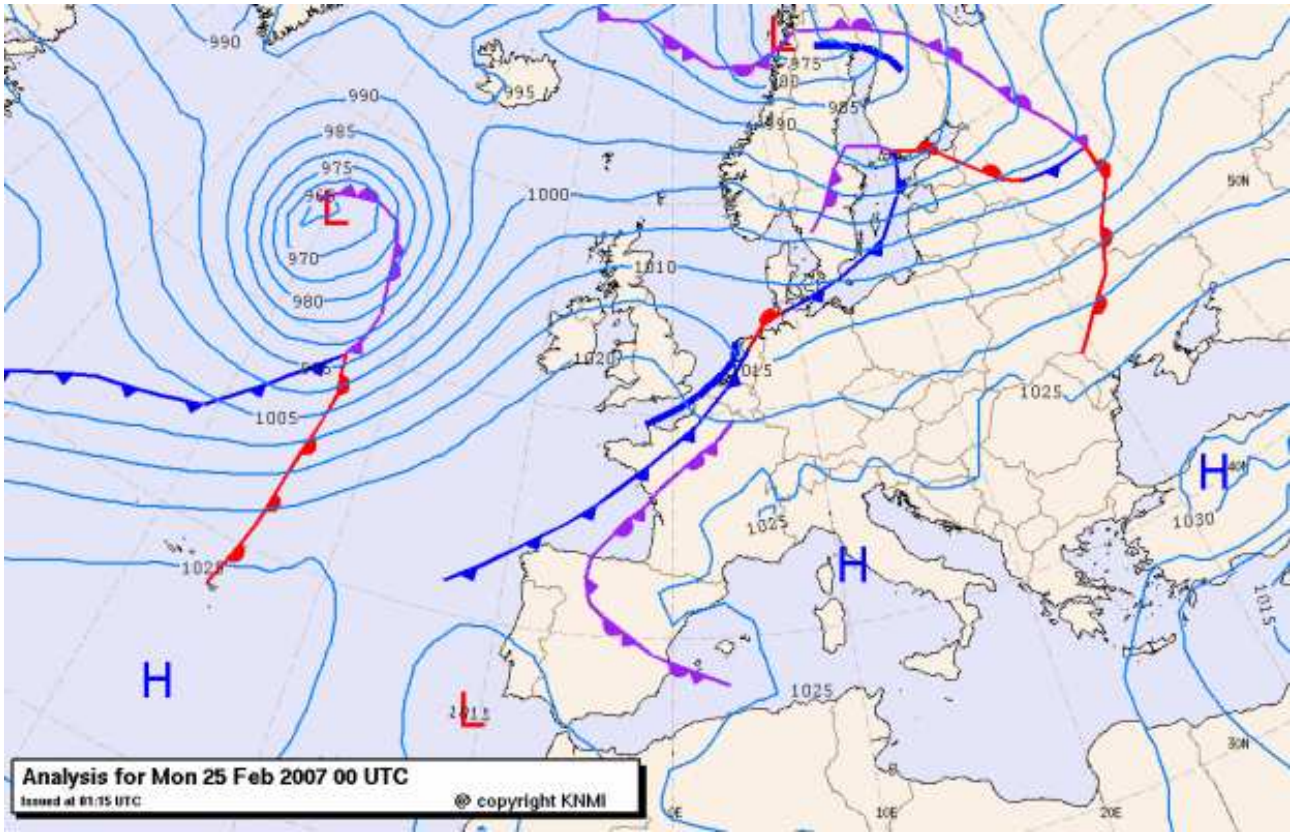


Figure 5.6: Analysis from KNMI based on HIRLAM analysis of February 25, 2008 00 UTC. .

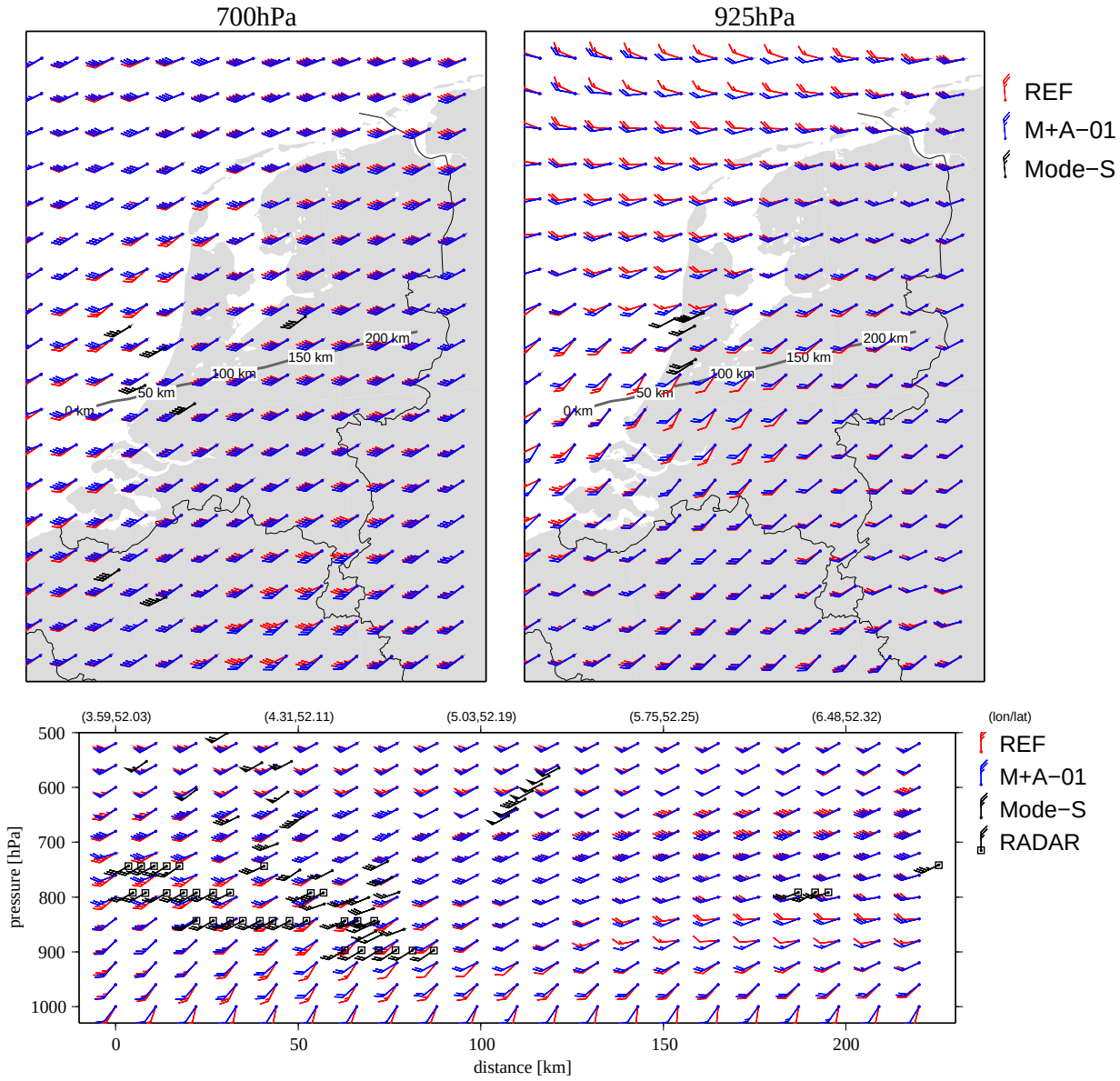


Figure 5.7: Wind fields for the REF- and M+A-01-run valid on 24 February 21 UTC. The squares denote the dual-radar wind observations at 1, 1.5, 2, and 2.5 km. In black are Mode-S observations.

vertical cross-section along the line displayed in the top panels. In this panel, besides the model wind vectors from the REF- and M+A-01 run, dual-radar wind and Mode-S observations are shown. The M+A-01-run matches better with both Mode-S and radar wind.

Figure 5.8 shows the horizontal wind at 700hPa and 925hPa, together with a vertical cross-section at 25 February, 00 UTC. At this time a few Mode-S observations were available and a

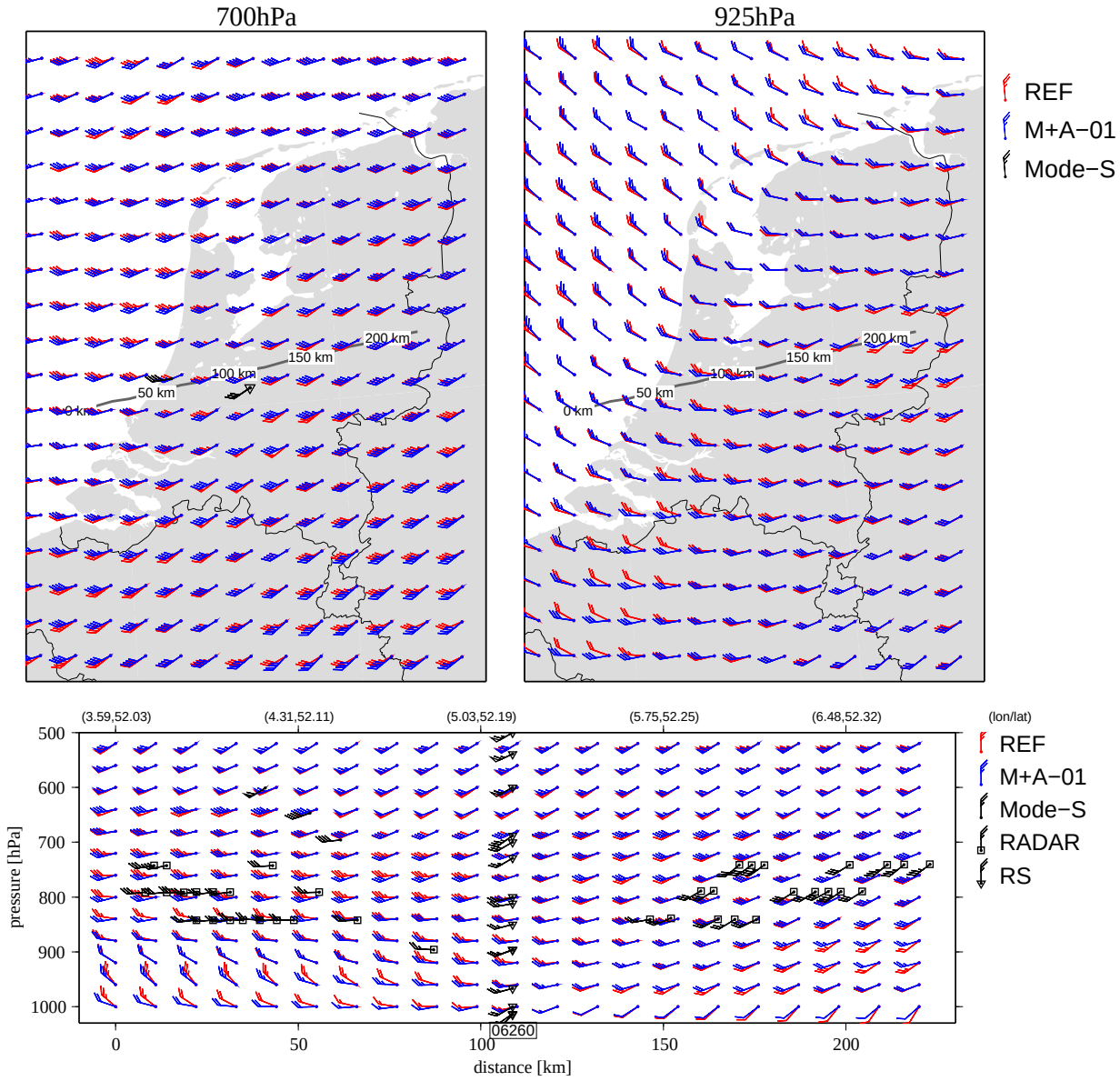


Figure 5.8: Wind fields for the REF- and M+A-01-run valid on 25 February 00 UTC. The squares denote the dual-radar wind observations at 1, 1.5, 2, and 2.5 km. In black are Mode-S observations and the inverse triangles are radiosonde observations from 06260.

radiosonde was launched at De Bilt. The model winds at 700hPa are close, while for 925hPa the REF-run the wind has shifted more to the north in the southern part of the Netherlands.

Some rain was associated with the passage of the cold front and and dual-doppler wind observations could be obtained. Behind the cold front (distance lower then 75km along the line), the M+A-01-run agree better with the observed dual-radar wind. Before the cold front

(distance 150km and further along the line) both model runs match the dual-radar wind. The radiosonde observations also agree with both models.

In summary, M+A-01 lies closer to independent dual-radar wind observations than REF, while both model runs match Mode-S and radiosonde observations.

## 5.3 29 February 12 UTC - 18 UTC

South of Greenland, a low pressure system, which deepened rapidly, moved eastward and was located west of Norway on the 29 February. During the 29 February, a warm front passed over the Netherlands in the evening and produced rain. The wind increased to stormy near the Dutch coast.

At 29 February, 12 UTC, both model-runs were in line with each other and with the observations (see Figure 5.10). The upper air flow was from the north-west, while at the surface a south-westerly flow was present. Also at 29 February 18 UTC (Fig. 5.11), both models were in line with observations (radiosonde, Mode-S and dual-radar winds) and each other. Note that around 770hPa the dual-radar winds seem to be inconsistent, most likely due to problems in the dual-radar wind retrieval (ambiguity problem or signal to noise degradation)

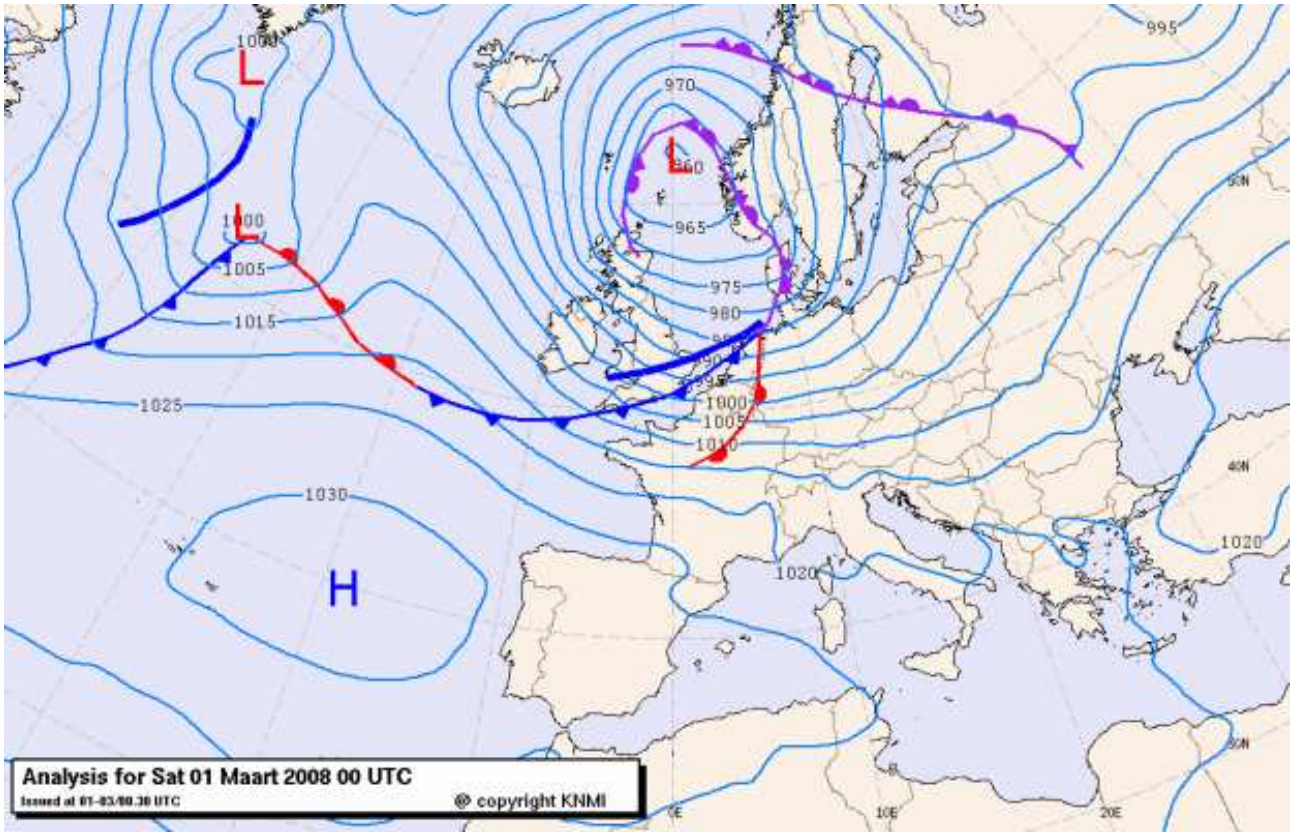


Figure 5.9: Analysis from KNMI based on HIRLAM analysis of March 01, 2008 00 UTC.

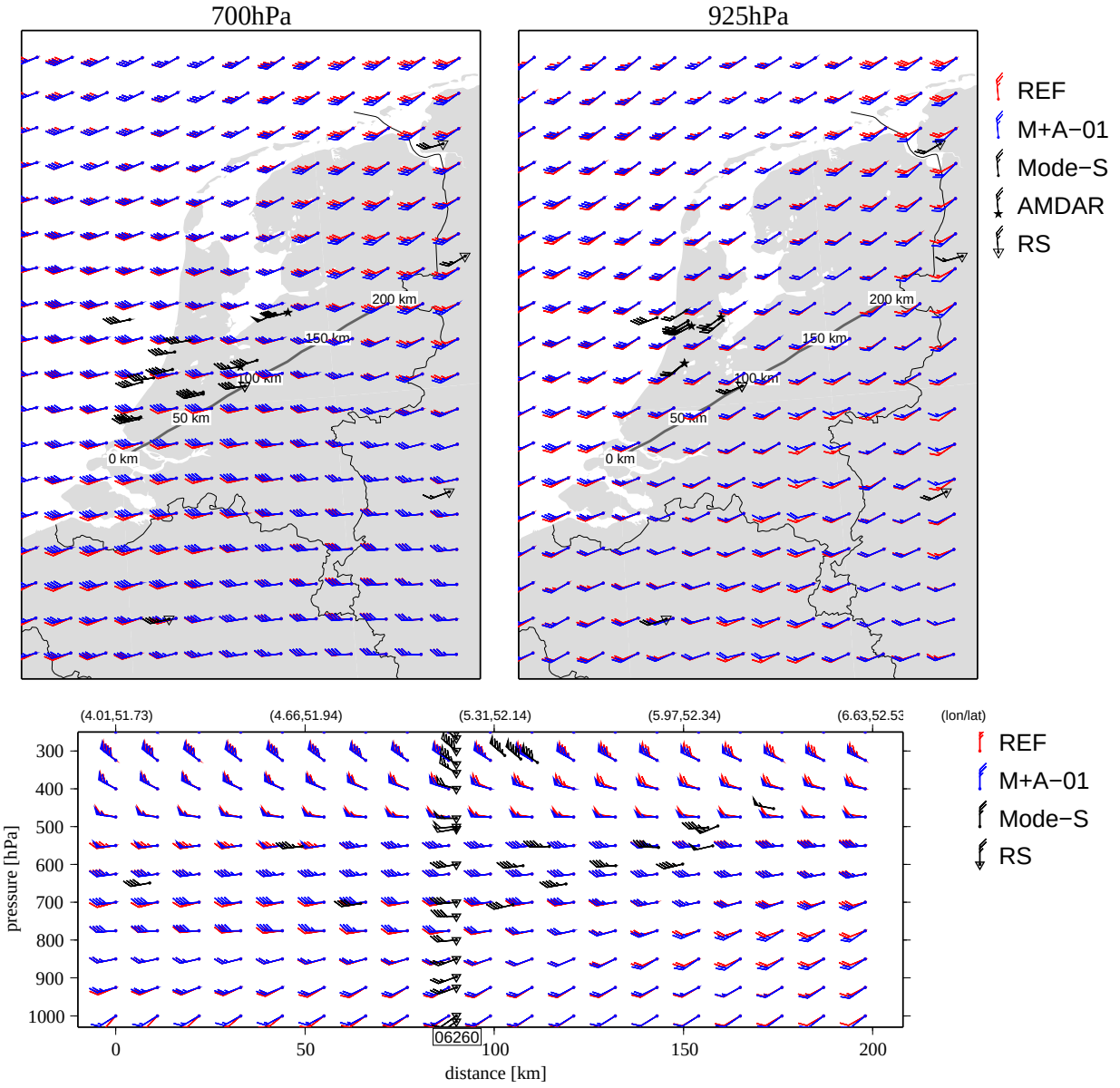


Figure 5.10: Wind fields for the REF- and M+A-01-run valid on 29 February 12 UTC. The inverse triangles are radiosonde observations from De Bilt (06260). In black are Mode-S observations.

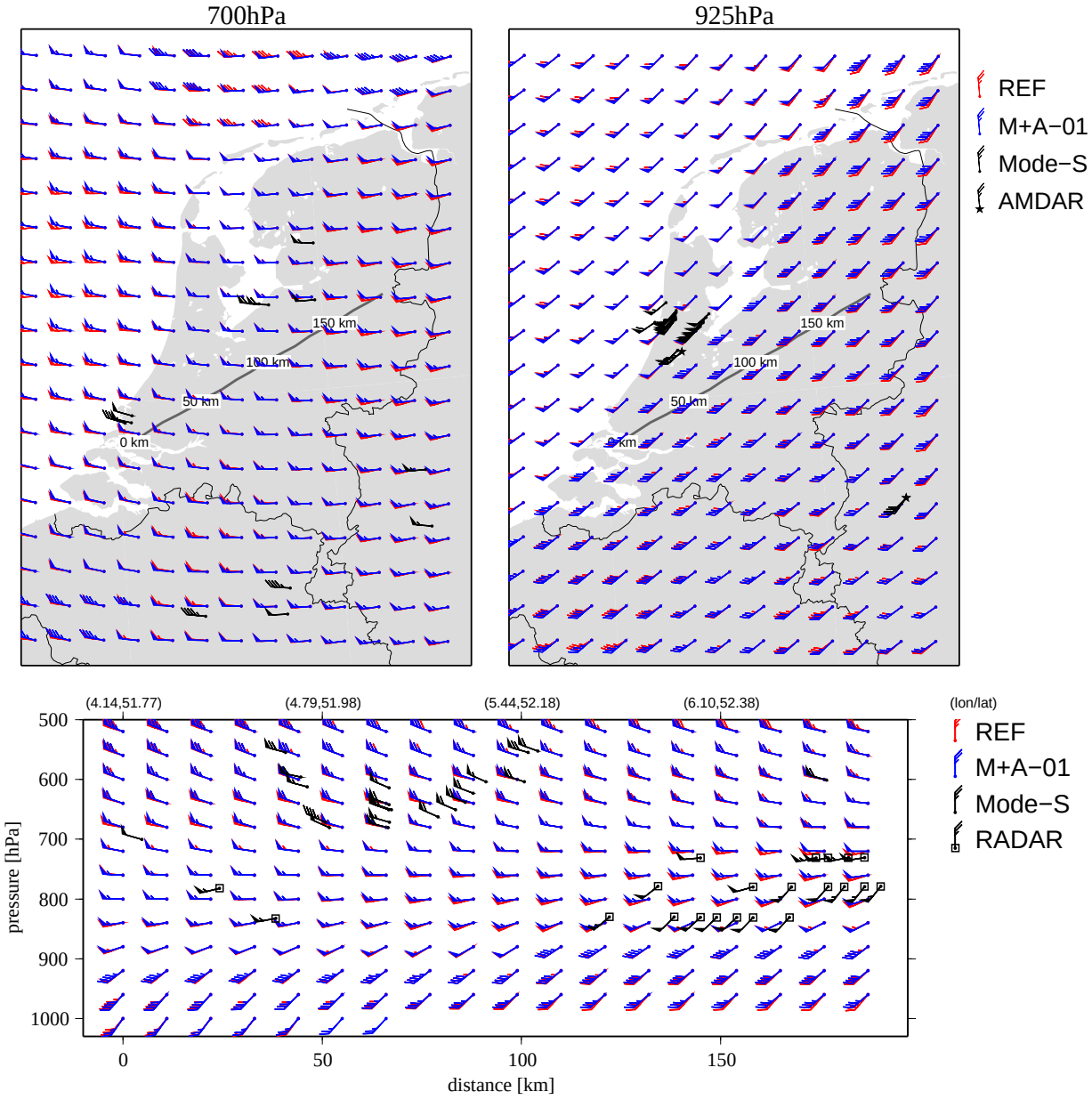


Figure 5.11: Wind fields for the REF- and M+A-01-run valid on 29 February 18 UTC. The squares denote the dual-radar wind observations at 1, 1.5, 2, and 2.5 km. In black are Mode-S observations.

## 5.4 4 March

On 4 March 2008, the general flow was from the North Sea bringing showers, some with snow. Figure 5.13 shows the model wind fields for 700hPa and 925hPa for March 4, 03UTC. The wind fields differ mostly near the coast of the Netherlands and over the western part of Belgium for 925hPa. For 700hPa, differences are observed in the north and south. Note that the radiosonde observation in De Bilt matches the M+A-01 better than the reference run. The differences between the model wind fields are also clearly visible along the vertical cross-section. The M+A-01 wind field lies closer the the observed dual-radar winds.

Figure 5.14 the wind at 400Pa and 500hPa is shown for March 4, 21UTC. It appears that the model forecast show a northerly flow over the Netherlands, but a clear wind shift to more north-westerly wind in the south-east of the area plotted in Figure 5.14. This wind shift is not present at 400 hPa (both experiments) and more extreme for M+A-01 at 500 hPa. At 700hPa, the location of the wind shift is more south for the REF-run than for the M+A-01-run.

From the cross section we see also that at a distance of approximately 250km REF has a more easterly flow with stronger winds (10-15 kts) than M+A-01. Unfortunately no quality can be assessed because no observations were present to compare to. Taking the observations into consideration, both model runs compare well to the observations.

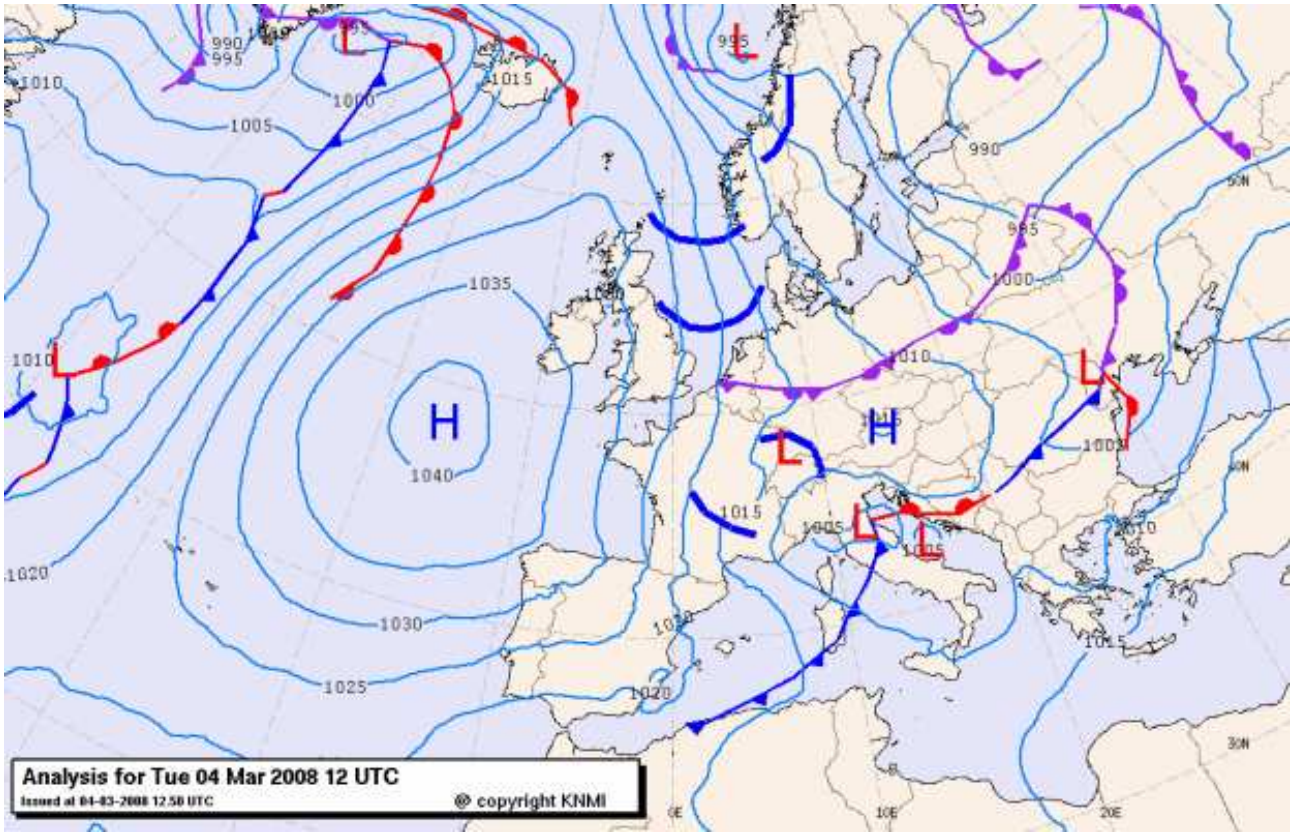


Figure 5.12: Analysis from KNMI based on HIRLAM analysis of 4 March 2008, 12 UTC.

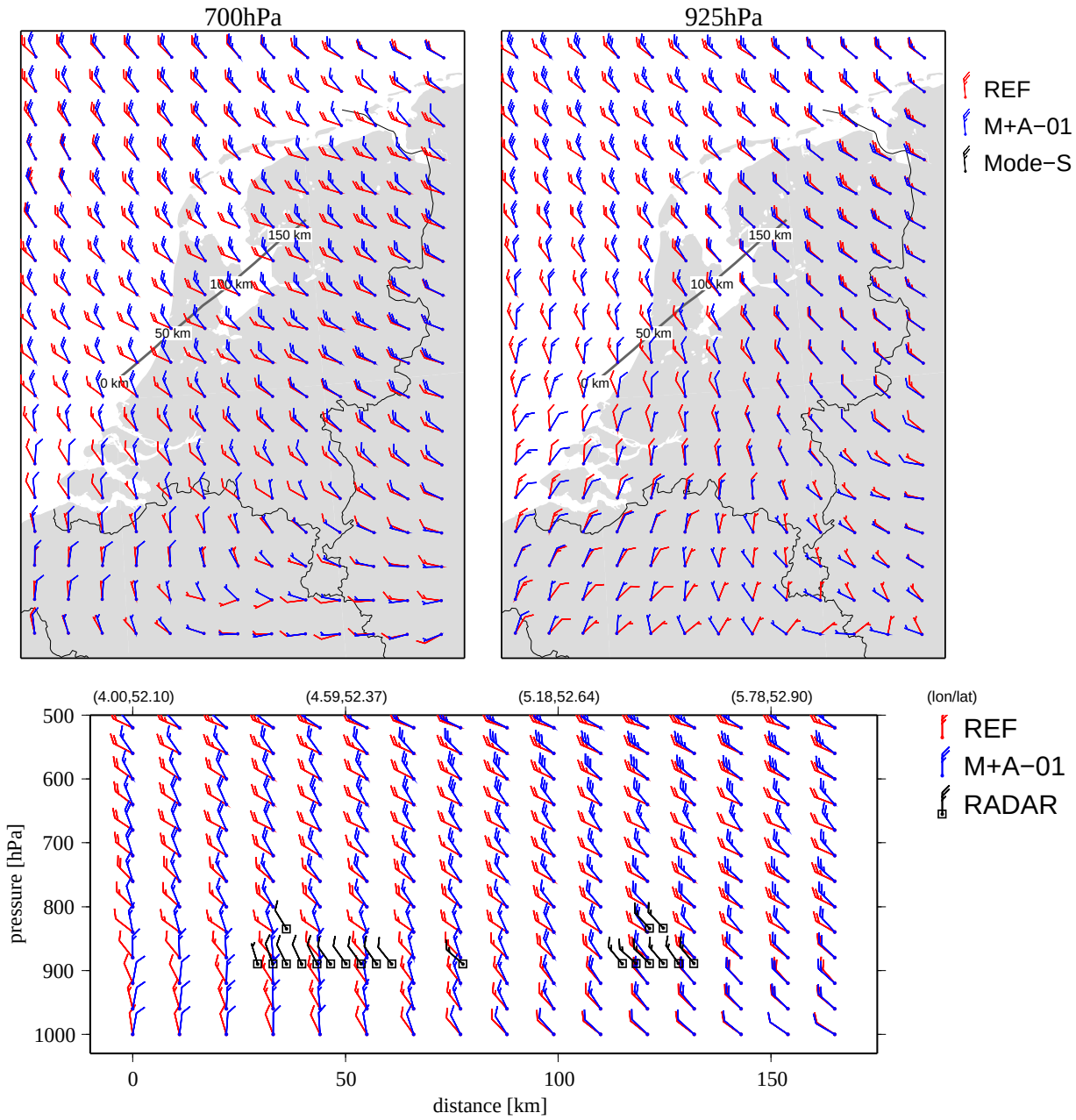


Figure 5.13: Wind fields for the REF- and M+A-01-run valid on 4 March 03 UTC. The squares denote the dual-radar wind observations at 1, 1.5, 2, and 2.5 km.

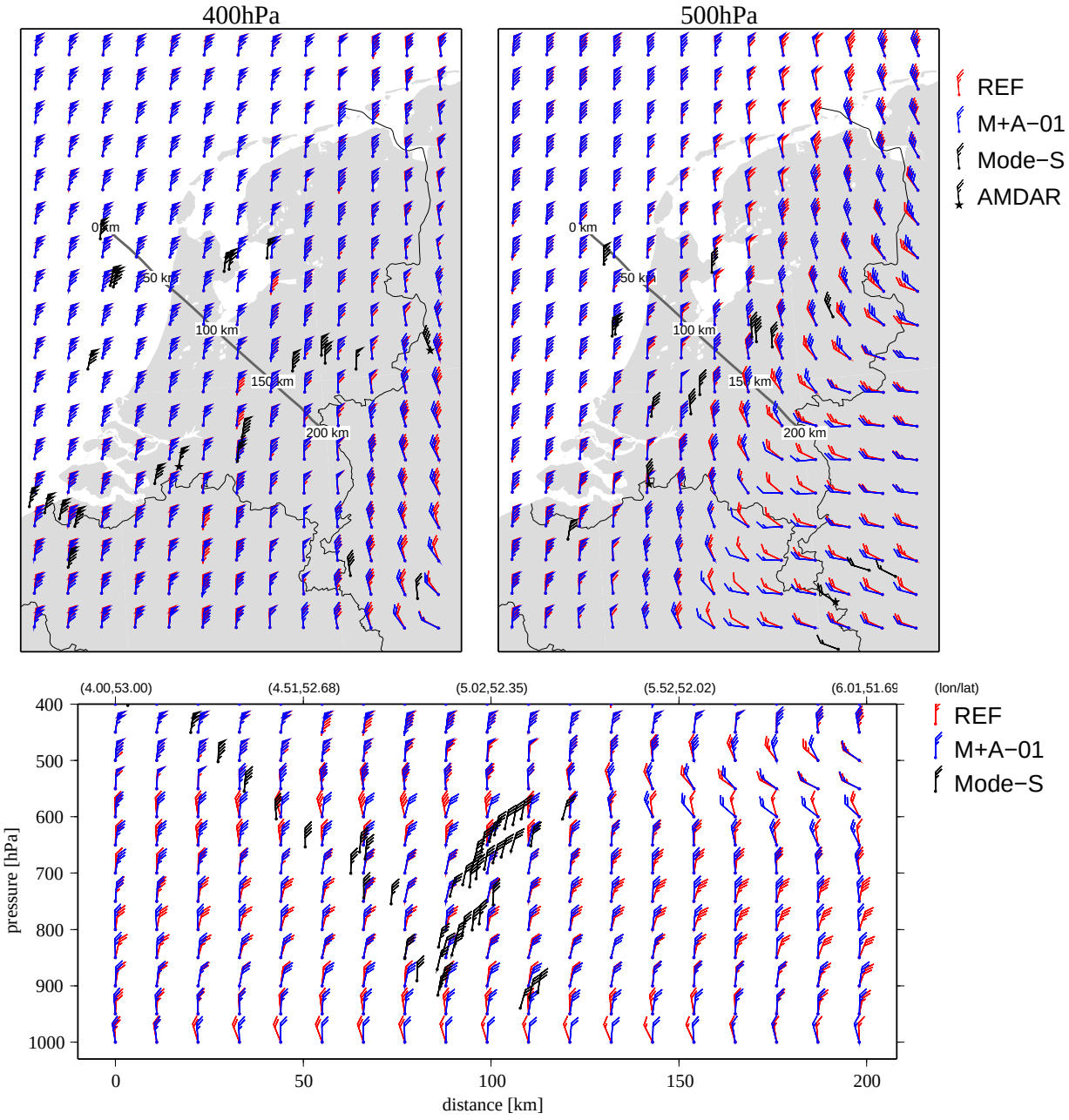


Figure 5.14: Analysis at 2008/03/04 21UTC of wind fields of the REF (red) and M+A-01 (blue) runs three pressure levels: 400hPa and 500hPa (top panels). Also shown in these panels are the Mode-S and AMDAR (stars) observations at these levels and times. Bottom panel shows the vertical cross section along the line displayed in the top panels.

In summary, M+A-01 is more in line with dual-radar observations which exhibit a more north westerly flow on Marh 4, 03 UTC. On 21 UTC, Mode-S observations show a northerly flow also observed in M+A-01, but less in REF.

## 5.5 10 March 12 UTC

The last case is from 2008/03/10. The general weather was governed disturbances which in a westerly flow dam from the Atlantic Ocean over Great Britain towards the North Sea, On March 10 an occluded front passed The Netherlands; this front was accompanied with rain and a strong winds. See Figure 5.15.

Figure 5.16 shows a general southerly flow. The main differences between the runs are located between 600hPa and 400hPa. Along the cross section, which runs now from approximately Uccle (Belgium) over De Bilt (The Netherlands) to the north of the Netherlands, the REF-run has at 600 hPa a more southerly wind which is not observed by the radiosonde observations from De Bilt and Uccle. These observations show a more westerly wind, which compares well with the M+A-01-run. At 600hPa an AMDAR observations over Belgium (see top panel) which reports a wind close to the M+A-01 run.

Around De Bilt there are differences between the radiosonde and REF at 400 hPa and

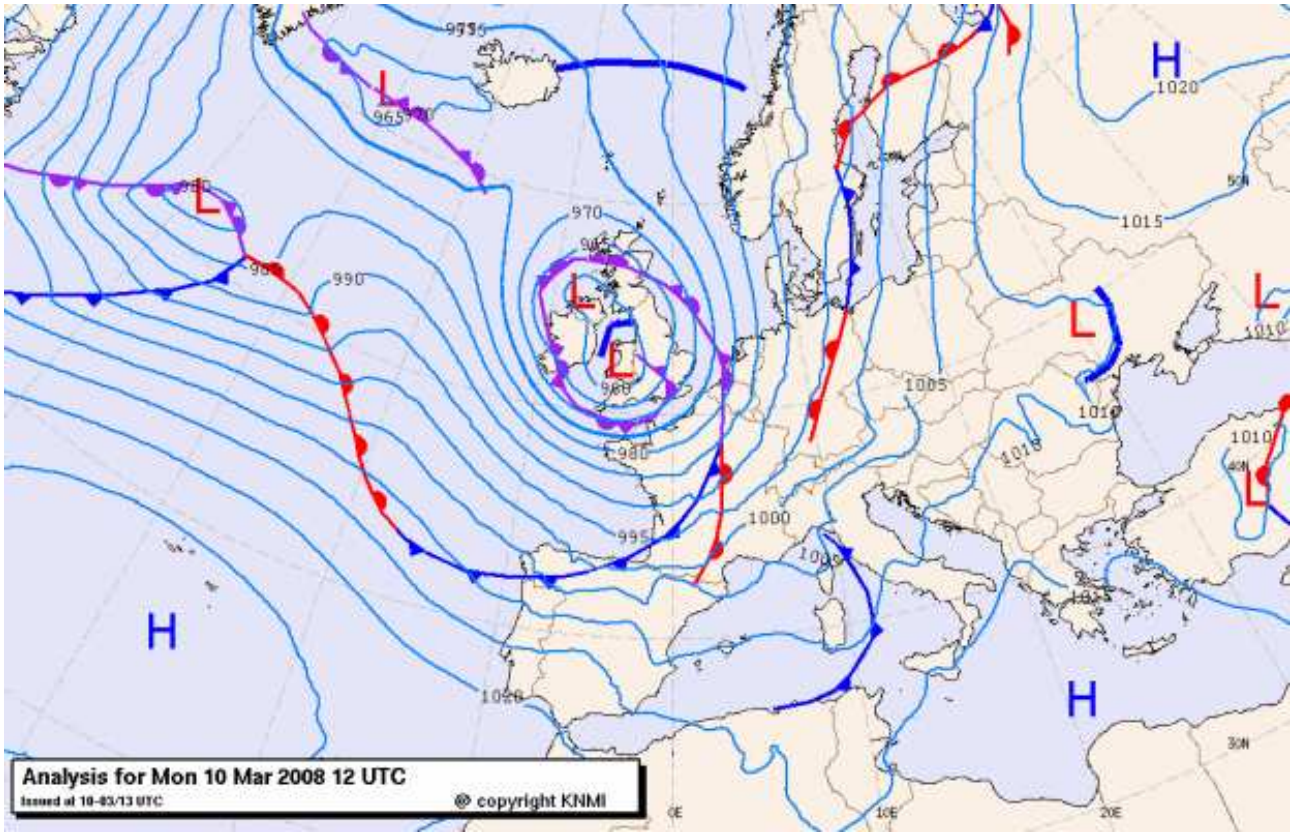


Figure 5.15: Analysis from KNMI based on HIRLAM analysis of March 10, 2008 12 UTC.

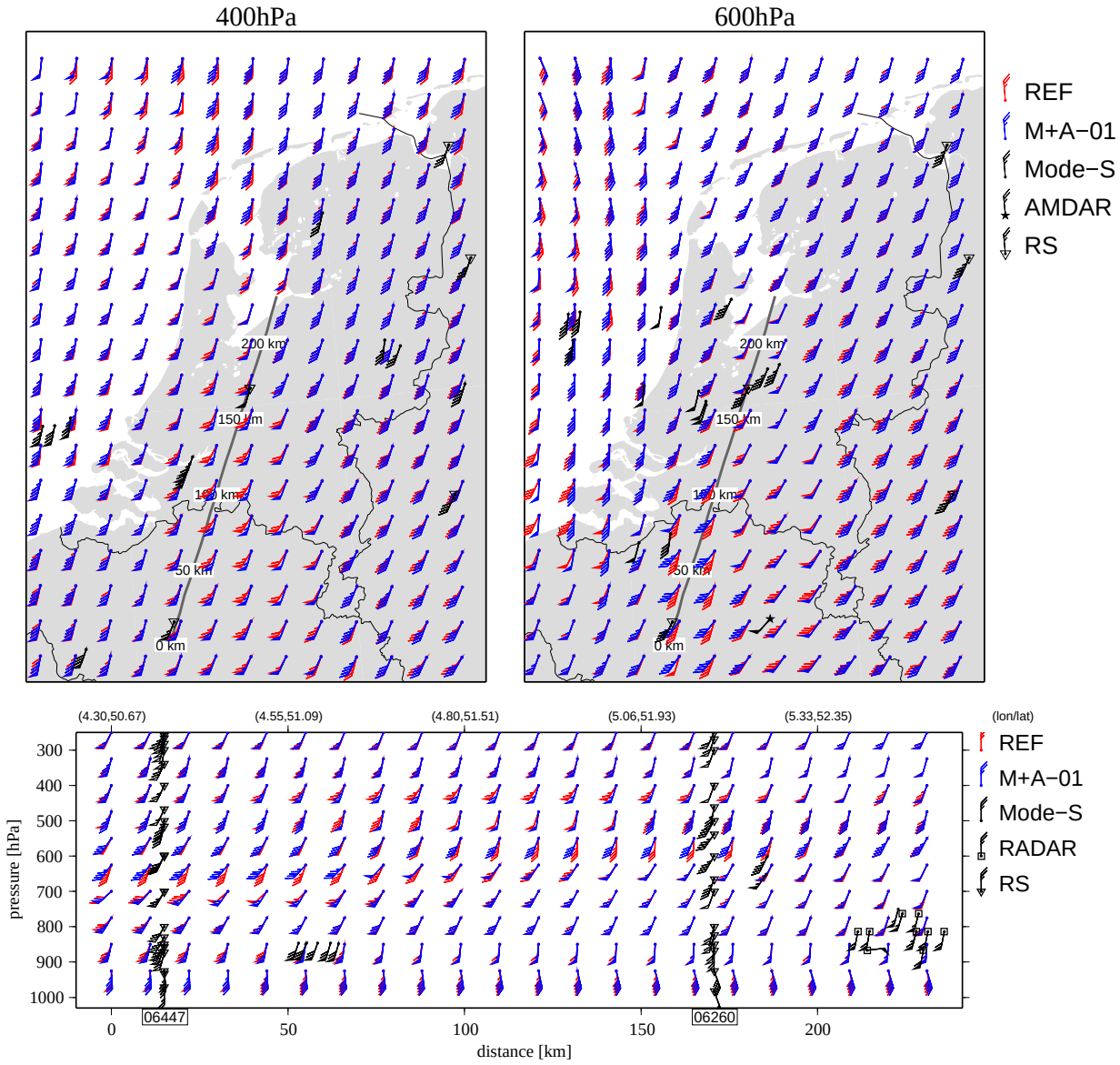


Figure 5.16: Same as previous figures but now for 2008/03/10 12UTC and levels 400hPa and 600hPa. Note that at this time radiosonde observations are available (denoted by inverse triangles).

550hPa: the observed wind speeds are around 10-15 kts, while the REF run is higher (for 400hPa) or lower (for 550hPa).

For this case, the wind observations seem to match the M+A-01 better than the REF run.

# Chapter 6

# Conclusions

The impact of timely, high spatial and temporal resolution aircraft observations available around Schiphol airport (De Haan, 2009) is tested on the nowcasting time scale in the HiRLAM numerical weather prediction (NWP) system (Undén et al., 2002) and is found generally beneficial.

Upper air observations, especially wind observations, are important for short-range weather forecasting of extreme weather and for meeting new requirements in aviation meteorology. To this end, in this report, a novel method of measuring wind and temperature from aircraft is discussed and assimilation in HIRLAM is carried out. All aircraft within a range of 275km of the Mode-S ("Mode-Selective") surveillance radar at Schiphol are polled every 4 seconds to extract observations of wind and temperature. The observations are accumulated in batches of 10 minutes and are available with almost no latency.

The impact is assessed by performing NWP experiments without and with the new data in the HIRLAM NWP model, configured to be close to the settings, boundaries and inputs used operationally at KNMI. The reported impacts are thus representative for KNMIs operational practice.

An hourly assimilation cycle is applied to exploit the high resolution (in space and time) of these new observations. Given the relatively small domain of the new observations we ran the experiments on a small HIRLAM domain after verifying negligible forecast impact of domain size over the forecast range of interest of 4 hours.

The general weather situation during the experiment from February 1, 2008, to March 10, 2008, was quite mixed with at times a well developed jet, a meandering flow and also including a blocked flow. As a result the impact statistics vary over time, but generally show a beneficial impact in the most variable (and uncertain) weather. Note however that the period used here was a winter period; for example summer periods with severe convection are not addressed in the impact experiment.

Verification of the forecasts with independent Mode-S aircraft observations shows clear analysis and short-range forecast impact. When the Mode-S observations, only available in a rather limited domain, are complemented with AMDAR aircraft observations, available over a large region, then a clear synergetic effect emerges of both data sources. On the other hand, the AMDAR observations on their own do not improve the analyses and forecasts. This is a clear indication that the availability of more airport surveillance radar aircraft observations would

further improve the analyses and forecasts in our area of interest (X11). A remaining puzzling result is the generally detrimental impact of AMDAR observations (without Mode-S) in the experiments. This could be due to the presence of observations near the domain boundary and/or poor coverage over the domain, especially around the Netherlands.

Verification with radiosondes at the De Bilt station confirm the above results. Although the analyses use the radiosonde information (at degraded resolution), it is revealing to see that the assimilation of Mode-S observations generally results in an improved fit of the analysis with the radiosonde observations. Radiosonde and Mode-S observations thus act complementary in the data assimilation system.

Statistics of observation minus background and observation minus analysis indicate that Mode-S aircraft observations are weighted relatively high with respect to the background field. This is in line with expectation and due to the high spatial and temporal density of the observations. The high spatial and temporal density does however offer the possibility to compute background error correlation structure based on the actual weather condition. This will be elaborated in a further study with the Mode-S data. In this report, the HIRLAM background and Mode-S observation error statistics were not modified to cope with these large observation densities. Therefore it is encouraging to see the high analysis impact in combination with beneficial forecast impact of Mode-S observations in an hourly assimilation cycle.

Case studies confirm the beneficial impact of Mode-S and illustrate the benefits in particular weather conditions.

Comparison with observations in real time of forecast fields show a decrease in wind speed and wind direction RMS of nearly 5% over the whole profile when the assimilation cycle is increased from once per three hours to once per hour. Implementation of an hourly cycle leads to a clear enhancement in forecast skill.

# Chapter 7

# Future Plans

Based on the results presented in this report we recommend to

- implement hourly system for nowcasting at KNMI since clear benefit is shown,
- arrange availability of more surveillance radar systems over extended area, since it is shown that additional aircraft data from surrounding area's improve the forecast at +03 and further,
- investigate the assimilation impact of other timely high-resolution data sources, such as rain radar winds, satellite EARS and GPS, and
- use Mode-S data to test model error structures depending on weather. Exploit this knowledge for better observation and background error settings, including error correlation settings.

## Acknowlegdements

The authors would like to thank LVNL for provision of the data. The time and effort of Gerrit Burgers and Sander Tijm (both KNMI) spend in reading and giving feedback on this report is highly appreciated.

This study has been carried out in close cooperation with the Knowledge & Development Centre Mainport Schiphol in The Netherlands (KDC, `http://www.kdc-mainport.nl`).

# Bibliography


Benjamin, S. G., and K.A. Brewster, and R. Brummer, and B. F. Jewett, and T. W. Schlatter, and T. L. Smith, and P. A. Stamus, 1991: An Isentropic Three-Hourly Data Assimilation System Using ACARS Aircraft Observations, *Monthly Weather Review*, **119**, 888–906.

Benjamin, S. G., and B. D. Jamison, and W. R. Moninger, and S. R. Sahm, and B. E. Schwartz, and T. W. Schlatter, 2010: Relative short-range forecast impact from aircraft, profiler, radiosonde, VAD, GPS-PW, METAR and mesonet observations via the RUC hourly assimilation cycle, *Monthly Weather Review*, **preprint**, 0000–0000.

Berre, L., 2000: Estimation of Synoptic and Mesoscale Forecast Error Covariances in a Limited-Area Model, *Monthly Weather Review*, **128**, 644–667.

Graham, R. J., and S. R. Anderson, and M. J. Bader, 2000: The relative utility of current observation systems to global-scale NWP forecasts, *Quarterly Journal of the Royal Meteorological Society*, **126**, 2435–2460.

Haan, S. de, 2009: Quality assessment of high resolution wind and temperature observations from ModeS, *KNMI-WR-200907*, Royal Netherlands Meteorological Institute, `http://www.knmi.nl/bibliotheek/knmipubWR/WR2009-07.pdf`.

Moninger, William R., and Richard D. Mamrosh, and Patricia M. Pauley, 2003: Automated Meteorological Reports from Commercial Aircraft, *Bulletin of the American Meteorological Society*, **84**, 203–216.

Moninger, William R., and Stanley G. Benjamin, and Brian D. Jamison, and Thomas W. Schlatter, and Tracy Lorraine Smith, and Edward J. Szoke, 2009: Evaluation of Regional Aircraft Observations using TAMDAR, *Weather and Forecasting*, **preprint**, –.

Stoffelen, A., and M. Bonavita, and J. Eyre, and M. Goldberg, and H. Järvinen, and C. Serio, and J.-N. Thépaut, and V. Wulfmeyer, 2006: Developments on atmospheric sounding and wind profiling, *Position paper - post-eps*, EUMETSAT.

Undén, P., and L. Rontu, and H. Järvinen, and P. Lynch, and J. Calvo, and G. Cats, and J. Cuxart, and K. Eerola, and C. Fortelius, and J. Garcia-Moya, and C. Jones, and G. Lenderlink, and A. McDonald, and R. McGrath, and B. Navascues, and N. Nielsen, and V. Odegaard, and E. Rodriguez, and M. Rummukainen, and R. R oõm, and K. Sattler,

and B. Sass, and H. Savijärvi, and B. Schreur, and R. Sigg, and H. The, and A. Tijm, 2002: HIRLAM-5 scientific documentation, *Technical report*, HIRLAM-project, Norrköping, http://hirlam.org.

World Meteorological Organization, 2003: WMO AMDAR reference manual, *WMO-no.958*, WMO, Geneva, http://www.wmo.int.

World Meteorological Organization, 2004: Statement of guidance regarding how well satellites and in situ sensor capabilities meet wmo user requirements in several application areas, *WMO- TD No. 1052*, WMO, Geneva, http://www.wmo.int.

World Meteorological Organization, 2006: Implementation plan for the evolution of space and surface-based sub-systems of the GOS, *WMO- TD No. 1267*, WMO, Geneva, http://www.wmo.int.

World Meteorological Organization, 2008: Fourth WMO workshop on the impact of various observing systems on NWP, 19-21 May 2008, WMO, http://www.wmo.ch/pages/prog/www/OSY/Reports/NWP-4_Geneva2008_index.html.